In presenting the dissertation as a partial fulfillment of
the requirements for an advanced degree from the Georgia
Institute of Technology, I agree that the Library of the
Institute shall make it available for inspection and
circulation in accordance with its regulations governing
materials of this type. I agree that permission to copy
from, or to publish from, this dissertation may be granted
by the professor under whose direction it was written, or,
in his absence, by the Dean of the Graduate Division when
such copying or publication is solely for scholarly purposes
and does not involve potential financial gain. It is under-
stood that any copying from, or publication of, this dis-
sertation which involves potential financial gain will not
be allowed without written permission.

3/17/65
b

OPTICAL PROPERTIES OF SODIUM IN THE VACUUM ULTRAVIOLET

A THESIS

Presented to

The Faculty of the Graduate Division

by

John Clark Sutherland

In Partial Fulfillment

of the Requirements for the Degree

Doctor of Philosophy

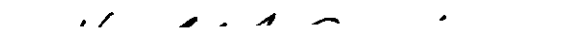in the School of Physics

Georgia Institute of Technology

May, 1967

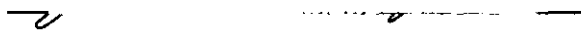OPTICAL PROPERTIES OF SODIUM IN THE VACUUM ULTRAVIOLET

Approved:

Chairman

Date approved by Chairman: *May 3 1967*

ACKNOWLEDGMENTS

I am indebted to the entire Radiation Physics Section of the Health Physics Division, Oak Ridge National Laboratory. In particular, I thank: E. T. Arakawa for directing my dissertation research, R. N. Hamm for writing the computer programs which I required, H. C. Schweinler and R. H. Ritchie for discussions of the theoretical aspects of my work and R. D. Birkhoff for his interest, encouragement, and enthusiasm. I also thank J. A. Harter and A. G. Kenerly for assistance in maintaining the electrical equipment used in the experiment. A special debt of gratitude is owed to Beverly Varnadore for her patient typing of the various drafts of this thesis and other papers and abstracts.

I thank J. R. Stevenson, Vernon Crawford and A. L. Stanford of the School of Physics, Georgia Institute of Technology, for the interest they showed in my work and the several trips they made to Oak Ridge. In addition, I am indebted to J. R. Stevenson for suggesting this research problem and to H. Gersch and J. W. Hooper for reading this thesis. I also thank Oak Ridge Associated Universities whose financial support made possible my work in Oak Ridge and in particular Louis Rayburn who made possible my attendance at several scientific meetings.

Special permission was received from the Graduate Division of the Georgia Institute of Technology to center page numbers in order to satisfy

the requirements for the Oak Ridge National Laboratory.

TABLE OF CONTENTS

LIST OF TABLES

LIST OF ILLUSTRATIONS

SUMMARY

Sodium is an excellent example of a free-electron metal. A striking feature of the optical properties of a metal of this type is its critical (or plasma) wavelength, λ_p. A free electron metal reflects almost all incident radiation of wavelength greater than λ_p, but is transparent to radiation of wavelength less than λ_p. Wood measured the reflectance of sodium in the ultraviolet and vacuum-ultraviolet regions of the spectrum and from these measurements estimated the plasma wavelength of sodium to be 2100 Å. Wood also showed that the transparent region extended to at least 500 Å. Skinner, using soft x-ray emission techniques, found the threshold for the excitation of core electrons at 405 Å. Thus the transparent region of sodium spans the vacuum-ultraviolet.

The real and imaginary parts of the complex index of refraction of sodium, $n^* = n + ik$, have previously been measured for photon wavelengths from 2537 Å to 25,000 Å (photon energies from 4.9 to .5 eV). The real and imaginary parts of the dielectric constant, $\epsilon^* = (n^*)^2$, agree with the quantum-mechanical theory of the optical constants of a nearly free-electron metal in this region except for the anomalous peak in the imaginary part of the complex dielectric constant, reported recently by Hodgson and also Mayer and co-workers for photon energies from 1.2 to 2.2 eV. This as yet

unexplained peak has caused considerable interest in the optical properties

of sodium.

The determination of the complex index of refraction of sodium in

its transparent region was undertaken so that the validity of the current

theory could be tested in this region. Also, the plasma wavelength, found

from the values of the real part of the complex dielectric constant, ϵ_1,

in the transparent region could be compared with the results of electron-

energy-loss experiments.

Radiation produced by a low pressure capillary-discharge tube was

dispersed by a Seya-Namioka type vacuum monochromator and reflected

from a sodium film. The films were formed by thermal evaporation of

sodium, whose purity exceeded 99.5%, from an electrically-heated tantalum

boat onto the flat surface of a quartz hemi-cylinder. The hemi-cylinder

was mounted on a rotatable sample holder inside an evacuated reflectance

chamber attached to the monochromator. Pressure in the reflectance

chamber during evaporation rose from 3×10^{-7} Torr to between 5×10^{-6}

and 2×10^{-5} Torr. Radiation reflected from the sodium film was detected

by a photomultiplier tube coated with sodium salicylate. The sample holder

and phototube were coupled together so that the reflectance of the film was

measured as a function of angle of incidence.

Two methods were used to measure the real part of the complex

index of refraction, n. The critical angle method was used to determine n

in the wavelength region from 950 Å to 2000 Å. This method makes use of

the fact that the index of refraction of sodium is less than 1.0 for photon

wavelengths less than λ_p. Hunter has shown that for sufficiently small

values of the imaginary part of the index of refraction, the critical angle

may be replaced by θ_m, the angle at which the rate of change of reflectance

with respect to the angle of incidence is a maximum, and thus

$$n = \sin \theta_m \quad .$$

Oxide which forms on the surface of the film which is exposed to vacuum

reduces the reflectance of this surface. However, both Hunter's

calculations and the reflectance of the unoxidized quartz-sodium interface,

measured for wavelengths from 2000 Å to the absorption edge of the quartz

at 1700 Å, show that the angle of maximum slope is not seriously affected

by the oxide.

Interference patterns observed for angles of incidence less than θ_m

were used to determine the index of refraction for photon wavelengths

from 420 Å to 1850 Å. The locations of interference maxima and minima

are given by

$$N\lambda = P\lambda + 2T (n^2 - \sin^2 \theta)^{\frac{1}{2}}$$

where λ is the wavelength of the incident radiation, N is the order of

interference, P is the net phase shift caused by reflections and trans-

missions at the surfaces of the films, T is the thickness of the film and θ

is angle of incidence of the interference maximum or minimum of order N.
A systematic method was developed to determine the proper order of
interference of each maximum and minimum. The value of P was computed
for each angle θ from the measured optical constants of the substrate and
the approximate optical constants of the sodium film. The value of n was
found by rewriting the interference equation in the form

$$\sin^2 \theta = n^2 - (\frac{\lambda}{2T})^2 (N - P)^2 \quad .$$

A straight line was fitted to the experimental values of $\sin^2 \theta$ and the
corresponding values of $(N - P)^2$ by the method of least squares. The value
of $\sin^2 \theta$ for $(N - P) = 0$ gave n. This value of n was used to recalculate P
and the process iterated. The values of n calculated in this way converged
rapidly.

Observations as a function of time of the interference pattern at a
given wavelength showed that while growth of the oxide layer on the vacuum-
sodium interface reduced reflectance, the locations of interference maxima
and minima were unchanged. Also, interference patterns for radiation
incident on the film through the quartz hemi-cylinder gave values of n
identical to those obtained when radiation was incident from the vacuum side
of the film. In addition there was good agreement between values of n
obtained by the critical-angle and interference methods.

The value of k was determined between 1746 $\overset{\circ}{A}$ and 2000 $\overset{\circ}{A}$ by
comparing the measured reflectances of the unoxidized quartz-sodium

interface as a function of incident angle with theoretical reflectances calculated from Fresnel's equations. Since k was found to be less than .04 in the region of interest it was possible to approximate $\epsilon_1 = n^2 - k^2$ by n^2 for all wavelengths less than 2000 Å, while $\epsilon_2 = 2nk$ could be computed only for the wavelengths at which k had been measured.

The theoretical expression for ϵ_1, derived from a model in which the electrons of the metal are described by Bloch wave functions, is related to the wavelength of the probing radiation, λ , by the equation

$$\epsilon_1 = 1 - \lambda^2/\lambda_a^2 + \delta\epsilon(\lambda)$$

where $\delta\epsilon(\lambda)$ is the contribution of interband transitions and λ_a is related to m_a, the average effective mass of a conduction band electron, and to $\varkappa_c$, the number of conduction electrons per unit volume, by

$$\lambda_a^2 = (\pi c^2/\varkappa_c e^2)m_a \quad .$$

Cohen has shown that when the range of wavelengths which can excite electrons in the conduction band to higher bands is sufficiently broad, $\delta\epsilon(\lambda)$ can be broken up into a constant term, and a term which goes as λ^2. Thus

$$\epsilon_1 = 1 + 4\pi\varkappa\alpha_1 - \lambda^2/\lambda_b^2$$

where $\varkappa$ is the number of atoms per unit volume, α_1 is intermediate between the total polarizability of an atom in the crystal, α_T, and the

polarizability of an ion core, α_o, and λ_b is related to the optical effective

mass of the conduction electrons, m_{opt}, by

$$\lambda_b^2 = (\pi c^2 / \varkappa_c e^2) m_{opt} \quad .$$

According to the calculated band structure of sodium, this equation should

be valid for radiation of wavelengths between the threshold for the direct

excitation of electrons in the conduction band at about 5600 Å ($\hbar\omega = 2.2$ eV)

and the threshold for the excitation of core electrons at 405 Å ($\hbar\omega = 30.8$

eV). The values of ϵ_1 determined in the present experiment were found to

be a linear function of λ^2 for wavelengths between 500 Å and 2000 Å in

agreement with theory. For λ less than 500 Å, the experimental values of

ϵ_1 were larger than the values predicted by Cohen's approximation. This

increase was attributed to the approach of the threshold for the excitation

of core electrons. The values of $1 + 4\pi\varkappa\alpha_1$ and m_{opt}/m determined from

the experimental data for wavelengths from 500 Å to 2000 Å were $1.03 \pm .02$

and $1.06 \pm .05$, respectively, where m is the mass of a free electron.

Mayer and Hietel found $1 + 4\pi\varkappa\alpha_1$ and m_{opt}/m to be $1.15 \pm .1$ and $1.17 \pm .03$,

respectively. The larger values found by Mayer and Hietel from measure-

ments made in the visible and near-ultraviolet wavelength regions are in

qualitative agreement with the nature of the approximations made in Cohen's

expression for ϵ_1. However, the value of $4\pi\varkappa\alpha_1$ determined in the present

work disagrees with the value of .13 found for $4\pi\varkappa\alpha_o$ by Tessman et al.

since according to theory $\alpha_0 < \alpha_1$. The present result is in somewhat better

agreement with the values of .07, .06, and .06 found for $4\pi\varkappa\alpha_0$ by Born and

Heisenberg, Fajans and Joos, and Pauling, respectively.

The plasma energy of sodium, $\hbar\omega_p$, found from the wavelength at

which ϵ_1 is equal to zero is 5.68 eV $\pm$ .06 eV. This value agrees well with

the values of 5.69 eV $\pm$ .08 eV, 5.67 eV $\pm$ .05 eV. 5.71 eV $\pm$ .1 eV, and

5.60 eV $\pm$ .05 eV determined in electron-energy-loss experiments by Robins

and Best, Swan, Kunz, and Sueoka, respectively.

CHAPTER I

INTRODUCTION

The first measurment of the optical constants of sodium was made

by P. Drude (1) in 1898. Using 5893 Å radiation, he found the index of

refraction of a molten sodium sample to be 0.0045. After allowing for

several possible errors, the index of refraction was found to be less than

0.054 at this wavelength. Even this larger value was quite small compared

with the indices of refraction of other metals.

In 1913 Duncan and Duncan (2) measured the optical constants of two

sodium samples at five wavelengths in the visible portion of the spectrum.

They solved the problem of obtaining an unoxidized sodium surface by filling

an evacuated glass cell with molten sodium, permitting the sodium to

solidify, and measuring the reflectance of polarized light from the glass-

sodium interface. Duncan and Duncan confirmed that the index of refraction

of metallic sodium was of the order of .05 throughout the visible portion of

the spectrum. This meant that sodium possessed one of the highest known

reflectances. In 1919 Wood (3) reported that the reflectivity of sodium

decreased rapidly in the ultraviolet region and also that sodium was trans-

parent in this region. Later (4, 5) he estimated the onset of transparency

at 2100 Å, measured the reflectance of sodium in its transparent region at

1860 Å and 1940 Å, and suggested that the index of refraction of sodium could be determined from both its Brewster's angle and its critical angle in this wavelength region. Wood also observed interference between components of the incident radiation reflected from the front and rear surfaces of a potassium film as a function of radiation wavelength and film thickness. In 1938 (6) Wood and Lukens found that sodium and other alkali metals were transparent to radiation of wavelength as short as 500 Å.

Zener (7) explained the transparency of the alkali metals in the ultraviolet and their high reflectance in the visible portions of the spectrum as a consequence of the Drude-Lorentz-Kronig (8) free-electron model of metallic structure. He showed that transparency started at the wavelength for which the dielectric constant of the metal was zero. The value of this critical wavelength calculated from the free-electron theory was 2100 Å, in agreement with the value estimated by Wood. Kronig (9) extended Zener's treatment of the problem to include damping of the conduction electrons. He thus showed that reflectance of slightly less than 100 per cent was expected for wavelengths greater than the critical wavelength.

Shortly after Kronig's theory was presented, Ives and Briggs (10) measured the optical constants of sodium, potassium, rubidium, and cesium at eight wavelengths from the ultraviolet (2537 Å) into the visible region of the spectrum (5780 Å). Their measurements on sodium (all made on one evaporated film) were in reasonable agreement with the previous work of

Duncan and Duncan(2) in the visible region. Also, the optical constants of

sodium were in much better agreement with Kronig's theory than were the

optical constants of the other alkali metals.

In 1940 Skinner (11), using soft x-ray emission techniques, found the

threshold for the excitation of core (L_{III}) electrons of sodium to be 30.8 eV

or 405 Å. This threshold established the short-wavelength limit of the

transparent region.

In 1958 Cohen (12) analyzed Ives and Briggs' data in terms of a

quantum mechanical theory of the optical properties of a metal. This

theory took into account the periodic structure of the metallic crystal and

the ion-core electrons, in addition to the free or conduction-band electrons.

Agreement was found between theory and experiment for all four metals.

From the experimental data, Cohen deduced values for the ion-core

polarization, critical (or plasma) wavelength, and optical-effective mass

of the conduction electrons of each metal. The agreement between the

measured optical constants of sodium and Kronig's older theory was shown

to result from the fact that in sodium the polarizability of the ion core is

quite small and the optical-effective mass of a conduction band electron is

only slightly larger than the rest mass of an electron. Cohen also called for

measurement of the optical constants of the alkali metals in the infrared

region of the spectrum since in this region the effects of interband

transitions are independent of wavelength and can be combined with the

ion-core polarizability to give the total atomic polarizability of an atom in the metal.

The first measurements of the optical constants of sodium in the infrared (6,500 Å to 25,000 Å) were made by Hodgson (13). The experimental error in his work was too great to permit determination of the atomic polarizability, but he did find that the average effective mass of a conduction electron was 1.08 times the mass of a free electron. Hodgson also reported absorption for photon energies near 1.2 eV. This absorption could not be explained by direct interband transitions since the threshold for the optical excitation of conduction-band electrons had been determined from band structure calculations (14, 15, 16) to be about 2.2 eV. Hodgson suggested that the anomalous absorption might be due to phonon-aided optical excitation of the conduction electrons.

Mayer and his co-workers (17, 18, 19, 20, 21) have measured the optical properties of sodium, potassium, rubidium, and cesium from the ultra-violet to the infrared (2968 Å to 25,000Å) under ultrahigh-vacuum conditions. They confirmed the anomalous absorption in sodium and reported similar phenomena in the other metals. In addition, they showed that the anomalous absorptions are temperature dependent, giving added weight to Hodgson's suggestion that a phonon-aided process is involved. Mayer and Hietel (17, 20) also reported that the ratio of the effective mass of the conduction electrons of sodium to the mass of a free electron was 1.27 (compared to

Hodgson's value of 1.08) and the corresponding ratio for the optical effective mass was 1.17 (compared to Cohen's (12) value of 1.01). Several attempts have been made to explain the anomalous absorptions of the alkali metals theoretically (22, 23, 24, 25, 26, 27, 28). It has been pointed out (22) that Hodgson's explanation based on phonon-aided indirect transitions is invalid because of momentum space considerations. Nettel (28) has suggested a more complicated theory based on phonon-aided absorption which reproduces some of the features of the Mayer's experimental results for sodium. However, the infrared optical properties of sodium remain an unsolved problem.

The purpose of this research was to extend the measurements of the optical constants of sodium into the vacuum-ultraviolet region of the spectrum (i.e., the region in which sodium is transparent), and to compare the optical constants measured in this region with the optical constants measured in the near-ultraviolet, visible, and infrared regions, with the results of electron-energy-loss experiments, and with current theories of the optical properties of metals. Since present techniques of vacuum-ultraviolet spectroscopy preclude the use of ultrahigh vacuum and transmission optics, it was necessary to find methods suitable for the determination of the optical constants in this region.

CHAPTER II

THEORY

Optical Constants

The effect of an isotropic or cubic solid on electromagnetic radiation

of energy $\hbar\omega$ passing through it is specified by two parameters: the index of

refraction, n, and the extinction coefficient, k. The index of refraction is

defined as the ratio of the velocity of the radiation in vacuum to its phase

velocity in the solid. The extinction coefficient is defined such that the

amplitude of the radiation is reduced by a factor of exp ($-2\pi k$) when it

traverses a distance of one vacuum wavelength in the material. Thus the

equation of the y components of the electric intensity of radiation of

energy $\hbar\omega$ moving in the positive x direction through a material of index of

refraction n and extinction coefficient k is

$$E_y\,(x,t) = E_y^o \exp\left\{i\left(\frac{2\pi nx}{\lambda} - \omega t\right)\right\} \exp\left\{-\frac{2\pi kx}{\lambda}\right\} \tag{1}$$

or

$$E_y\,(x,t) = E_y^o \exp\left\{i\left(\frac{2\pi n^*x}{\lambda} - \omega t\right)\right\} \tag{2}$$

where

$$n^* = n + ik \tag{3}$$

is the complex index of refraction. Equation (2) is formally the same as the

equation for radiation passing through a transparent material.

The interaction between a solid and electromagnetic radiation may also be described by the dielectric constant and conductivity of the solid. In an isotropic or cubic solid the current density, J, and electric polarization intensity, P, are given by

$$J = \sigma E \tag{4}$$

and

$$P = \varkappa \alpha E \tag{5}$$

where σ is the conductivity, α is the polarizability of a single atom, and $\varkappa$ is the number of atoms per unit volume. If the solid is uncharged and magnetic effects can be ignored, Maxwell's equations for the solid are

$$\nabla \cdot E = 0 \tag{6}$$

$$\nabla \cdot H = 0 \tag{7}$$

$$\nabla \times E = -\frac{1}{c}\frac{\partial H}{\partial t} \tag{8}$$

$$\nabla \times H = \frac{(1 + 4\pi\varkappa\alpha)}{c}\frac{\partial E}{\partial t} + \frac{4\pi\sigma}{c} E \quad . \tag{9}$$

From equation (1)

$$\frac{\partial E}{\partial t} = - i\omega E \tag{10}$$

so equation (9) can be written

$$\nabla \times H = (1 + 4\pi\varkappa\alpha + i\frac{4\pi\sigma}{\omega})\frac{1}{c}\frac{\partial E}{\partial t} \tag{11}$$

or

$$\nabla \times H = \frac{\epsilon^*}{c}\frac{\partial E}{\partial t} \tag{12}$$

where $\epsilon^* = \epsilon_1 + i\epsilon_2$ is the complex dielectric constant. The real part of the complex dielectric constant, $\epsilon_1 = 1 + 4\pi\varkappa\alpha$, gives the polarizability of the

material, while the imaginary part, $\epsilon_2 = \dfrac{4\pi\sigma}{\omega}$, is related to the rate of

absorption of energy by the material since the mean power absorbed per

unit volume is $\overline{J \cdot E}$ or $\overline{\sigma E^2}$. Substitution of expressions of the form of equation

(2) for E and H in equations (8) and (11) shows that

$$\epsilon^* = (n^*)^2 \tag{13}$$

or

$$\epsilon_1 = n^2 - k^2 \tag{14}$$

and

$$\epsilon_2 = 2nk \quad . \tag{15}$$

Optical Properties of Metals

The parameter ϵ^* describes the macroscopic interaction of a solid and

electromagnetic radiation. Expressions for ϵ^* in terms of microscopic

parameters can be derived from models of the structure of the solid. The

first theory of the optical properties of metals was based on Drude's (29)

free-electron model of metallic structure and used classical mechanics. The

next theory was based on an independent-particle quantum-mechanical model

using Bloch wave functions (12, 30, 31). The most recent theory is that of

Bohm and Pines (32, 33) which includes electron-electron interactions.

In Drude's free-electron model (29, 30) the only forces acting on the

valence electrons of a metal are due to impressed electric fields and viscous

damping. Thus the differential equation of motion for the y coordinate of

an electron is

$$m \frac{\partial^2 y}{\partial t^2} = - e E_y (x, t) - 2\pi m\gamma \frac{\partial y}{\partial t} \tag{16}$$

where e and m are respectively the charge and mass of the electron, $2\pi m\gamma$

is the damping constant and E_y is the time varying electric intensity given

by equation (2). The steady state solution to equation (16) is

$$y (x, t) = \frac{e/m}{\omega^2 + i \, 2\pi\gamma\omega} \quad . \tag{17}$$

The complex polarization, $P_y (x, t)$ and the electric intensity, $E_y (x, t)$, are

related by

$$P_y (x, t) = \frac{(\epsilon^* - 1)}{4\pi} E_y (x, t) \quad . \tag{18}$$

However

$$P_y (x, t) = -\varkappa_c \, e \, y (x, t) \tag{19}$$

where $\varkappa_c$ is the number of conduction electrons per unit volume. Substituting

equation (17) for $y (x, t)$ and separating real and imaginary parts gives

$$\epsilon_1 = 1 - \frac{(4\pi\varkappa_c \, e^2/m)}{\omega^2 + 4\pi^2\gamma^2} \tag{20}$$

and

$$\epsilon_2 = (4\pi\varkappa_c \, e^2/m) \frac{2\pi\gamma}{\omega(\omega^2 + 4\pi^2\gamma^2)} \quad . \tag{21}$$

The quantity $4\pi\varkappa_c e^2/m$ is abbreviated ω_o^2. The value of $2\pi\gamma h$, estimated

from the static conductivity of sodium (34), is .02 eV. So, for photon

energies much greater than .02 eV, equations (20) and (21) become

$$\epsilon_1 = 1 - \omega_o^2/\omega^2 \tag{22}$$

and

$$\epsilon_2 = 2\pi\gamma \omega_o^2/\omega^3 \quad . \tag{23}$$

The quantum mechanical theory of the optical properties of metals

based on an independent-particle model has been reviewed by Seitz (30),

Fröhlich (31), and Cohen (12). According to this model

$$\epsilon_1 = 1 - \frac{4\pi e^2}{m\omega^2} \sum_s \frac{2}{(2\pi)^3} \int d^3\underline{\kappa} \, f_{s\underline{\kappa}, s\underline{\kappa}} \qquad (24)$$

$$+ \frac{4\pi e^2}{m} \sum_s \sum_r \frac{2}{(2\pi)^3} \int \frac{d^3\underline{\kappa} \, f_{r\underline{\kappa}, s\underline{\kappa}}}{\omega_{r\underline{\kappa}, s\underline{\kappa}}^2 - \omega^2}$$

and

$$\epsilon_2 = \frac{2\pi^2 e^2}{m\omega} \sum_s \sum_r \frac{2}{(2\pi)^3} \int d^3\underline{\kappa} \, | f_{r\underline{\kappa}, s\underline{\kappa}} | \delta(\omega - \omega_{r\underline{\kappa}, s\underline{\kappa}}) \qquad (25)$$

where $\underline{\kappa}$ is the wave vector of an electron and $f_{a\underline{\kappa}_1, b\underline{\kappa}_2}$ is the oscillator-

strength density for a transition from state $\underline{\kappa}_2$ in band b to state $\underline{\kappa}_1$ in band

a. If the wavelength of an incident photon is large compared to the

dimensions of a unit cell, the momentum of the photon is much less than the

momentum of an electron in the crystal. Thus, for optically induced inter-

band transitions in which phonons are not involved, $\underline{\kappa}_1$ is equal to $\underline{\kappa}_2$. Direct

interband transitions are illustrated by Figure 1 which shows the calculated

values of the energy of the electronic states of metallic sodium (14, 15, 16)

as a function of $\underline{\kappa}$ for values of $\underline{\kappa}$ lying along a Σ -axis between the origin

Γ and the Brillouin zone boundary N. The bands shown in the figure are,

from bottom to top, the L_3 band which is part of the ion-core of metallic

sodium, the conduction band which is filled only to the Fermi energy, E_F, the first unoccupied band, three higher unoccupied bands, and a portion of a fourth unoccupied band. Interband transitions are shown in Fig. 1 as arrows from a state described by a wave-vector $\underline{K}$ and a band index to another state described by the same value of $\underline{K}$ and a different band index. The first state must lie below E_F, while the second state must lie above E_F.

The oscillator-strength density for an interband transition is a function of the momentum-matrix elements connecting the initial and final states, and of their energy difference, i. e.

$$f_{r\underline{K}, s\underline{K}} = \frac{2}{3m} \frac{\langle r\underline{K} | \underline{p}^{op} | s\underline{K} \rangle \cdot \langle s\underline{K} | \underline{p}^{op} | r\underline{K} \rangle}{E_{r\underline{K}} - E_{s\underline{K}}} . \tag{26}$$

The term $\omega_{r\underline{K}, s\underline{K}}$ in equations (24) and (25) is defined by

$$\hbar \omega_{r\underline{K}, s\underline{K}} = E_{r\underline{K}} - E_{s\underline{K}} . \tag{27}$$

The term $f_{s\underline{K}, s\underline{K}}$ in equation (24) is the oscillator-strength density connecting a state in a filled band with itself and is given by

$$f_{s\underline{K}, s\underline{K}} = \frac{m}{3\hbar^2} \nabla_{\underline{K}}^2 E_{s\underline{K}} . \tag{28}$$

In general $f_{s\underline{K}, s\underline{K}}$ must be summed over all occupied states. However, in sodium the highest core level (L_3 in Fig. 1) lies 28 eV below the bottom of the conduction band and is independent of $\underline{K}$ as are the other core bands
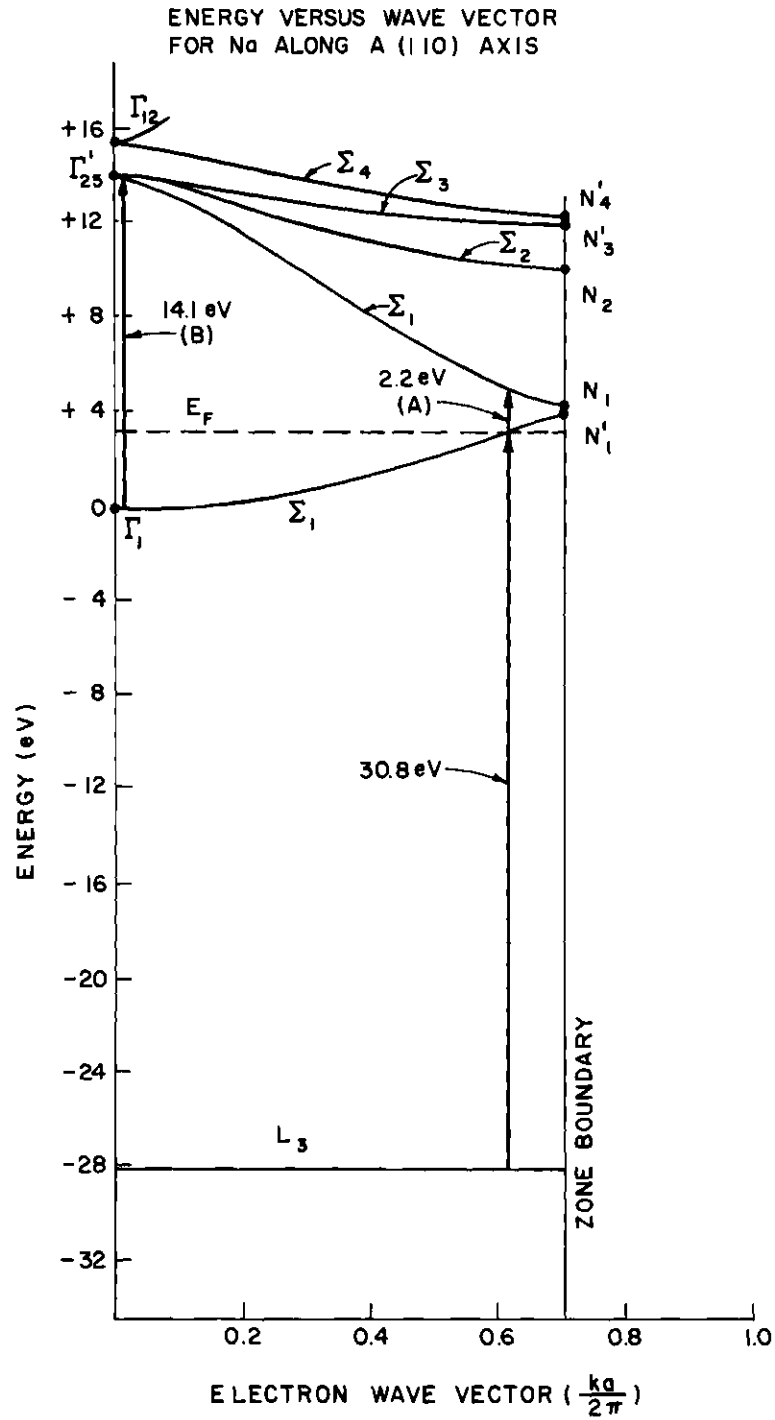
Figure 1. Energy Versus Wave Vector for Sodium along a (1, 1, 0) Axis

which lie still further below the conduction band. Thus for sodium the second

term in equation (24) reduces to

$$\frac{4\pi e^2}{m\omega^2} \frac{2}{(2\pi)^3} \int d^3\kappa \, f_{c\underline{\kappa}, c\underline{\kappa}} \tag{29}$$

where the index c denotes the conduction band. In general, however, the

summation over filled bands in the second term in equation (24) must include

all bands whose energy is dependent on $\underline{\kappa}$. Thus, for example, in the case of

gold the conduction band and the d bands would be included since the latter

lie just below the Fermi energy and are dependent on $\underline{\kappa}$.

The conduction band contains both filled and empty states and thus

the band index c appears in both $\sum_s$ and $\sum_r$ in the third term of equation (24).

When c appears as the index of a filled band the integral over reciprocal space

is restricted to $\underline{\kappa}$ inside the Fermi surface, while if c appears as the index

of an empty band the integral is over the volume of reciprocal space between

the Fermi surface and the zone boundary. When neither the initial nor the

final state is in the conduction band, the integration is over the entire

Brillouin zone. The second term of equation (24) is affected only by the

filled states of the conduction band so the integration over reciprocal space

is restricted to $\underline{\kappa}$ inside the Fermi surface. The factor of 2 which appears

before each integral in equations (24) and (25) represents the result of

summation over spin states since the oscillator strengths are independent of

spin.

The first two terms in equation (24) give the contribution of the conduction band or "free" electrons to ϵ_1. These terms may be put in a form similar to the classical expression for ϵ_1, equation (22), by defining an effective mass of the conduction electrons, m_a, such that m/m_a is the average value of the conduction band oscillator strength, $f_{c\underline{K}, c\underline{K}}$, i. e.

$$\frac{m}{m_a} = \frac{2}{\varkappa_c (2\pi)^3} \int d^3 \underline{K} \, f_{c\underline{K}, c\underline{K}} \quad . \tag{30}$$

Then if

$$\omega_a^2 = \frac{4\pi\varkappa_c e^2}{m_a} \quad , \tag{31}$$

equation (24) becomes

$$\epsilon_1 = 1 - \frac{\omega_a^2}{\omega^2} + \delta\epsilon_1(\omega) \tag{32}$$

where $\delta\epsilon_1(\omega)$ is the contribution of interband transitions. Cohen (12) has pointed out that there are two cases for which simple approximations can be made for $\delta\epsilon_1(\omega)$. First, for photon energies less than the minimum energy required for interband transitions, i. e., $\hbar\omega$ less than the smallest value of $\hbar\omega_{r\underline{K}, s\underline{K}}$, $\delta\epsilon(\omega)$ is very nearly constant and equation (32) can be written

$$\epsilon_1 \doteq 1 + 4\pi\varkappa\alpha_T - \frac{\omega_a^2}{\omega^2} \tag{33}$$

where $\varkappa$ is the number of atoms per unit volume and α_T, the total polariza-bility of an atom in the crystal lattice, is given by

$$\alpha_T = \frac{e^2}{\kappa} \, m \sum_s \sum_r \frac{2}{(2\pi)^3} \int d^3\underline{\kappa} \, \frac{f_{r\underline{\kappa}, s\underline{\kappa}}}{\omega^2_{r\underline{\kappa}, s\underline{\kappa}}} \quad . \tag{34}$$

The lowest energy interband transition in sodium is labeled "A" in Figure 1. This is a transition from states just below the Fermi energy in the conduction band with wave vectors along a Σ-axis to states with the same wave vectors in the first unoccupied band. According to the band calculations, the energy of this transition is 2.2 eV. Thus according to the independent-particle model equation (33) should be valid for photon energies less than 2.2 eV but greater than .02 eV (cf. equations (20) and (22)). However, Mayer and Hietel (17, 20) and Hodgson (13) have reported anomalous absorption for energies between 1.2 and 2.2 eV. Thus equation (33) is valid only for photon energies between .02 eV and 1.2 eV.

If conduction band transitions are spread over a broad range of energy and if the corresponding oscillator strengths are not strongly energy dependent, another simple approximation can be made for $\delta \epsilon(\omega)$. In this approximation $\delta\epsilon(\omega)$ is divided into three terms: a sum over transitions from the core bands to unfilled bands, a sum over transitions from the conduction band to unfilled bands for which $\omega_{r\underline{\kappa}, c\underline{\kappa}} > \omega$; and a sum over conduction band transitions for which $\omega_{r\underline{\kappa}, c\underline{\kappa}} < \omega$. In the first two terms ω is equated to zero while in the third term $\omega_{r\underline{\kappa}, c\underline{\kappa}}$ is equated to zero. Thus equation (32) becomes

$$\epsilon_1 \doteq 1 + 4\pi\varkappa\alpha_o + \frac{4\pi e^2}{m} \sum_{\omega_{r\underline{K},c\underline{K}} > \omega} \frac{2}{(2\pi)^3} \int d^3 \underline{K} \frac{f_{r\underline{K},c\underline{K}}}{\omega^2_{r\underline{K},c\underline{K}}} \qquad (35)$$

$$-\frac{\omega^2_a}{\omega^2} - \frac{4\pi e^2}{m\omega^2} \sum_{\omega_{r\underline{K},c\underline{K}} < \omega} \frac{2}{(2\pi)^3} \int d^3 \underline{K} \, f_{r\underline{K},c\underline{K}}$$

where the polarizability of the core electrons, α_o, is given by

$$\alpha_o = \frac{e^2}{\varkappa} m \sum_{s \neq c} \sum_{r} \frac{2}{(2\pi)^3} \int d^3 \underline{K} \frac{f_{r\underline{K},c\underline{K}}}{\omega^2_{r\underline{K},s\underline{K}}} \qquad . \qquad (36)$$

The third term in (35) is nearly constant and may be combined with the

second term while the fifth term goes nearly as ω^{-2} and can thus be combined

with the fourth term to give

$$\epsilon_1 \doteq 1 + 4\pi\varkappa\alpha_1 - \frac{\omega^2_b}{\omega^2} \qquad . \qquad (37)$$

An effective-optical-electron mass, m_{opt}, defined in analogy with equation

(31) is given by

$$\omega^2_b = \frac{4\pi\varkappa_c e^2}{m_{opt}} \qquad . \qquad (38)$$

Comparison of equations (33), (35), and (37) shows that

$$m_a \geq m_{opt} \qquad (39)$$

and also

$$\alpha_T \geq \alpha_1 \geq \alpha_o \quad . \tag{40}$$

Equation (37) is valid if the range of energies for transitions from

filled states in the conduction band to empty states in higher bands is large.

The threshold for these transitions is 2.2 eV corresponding to transition "A"

in Figure 1. The highest energy transition between the conduction band and

the first unoccupied band occurs at Γ and has an energy of 14.1 eV. This

transition is labeled "B" in Figure 1. However, transitions from the

conduction band to other unoccupied bands start for photon energies of

5.3 eV and continue without interruption to energies greater than the

threshold for the excitation of core electrons which is 30.8 eV. Since the

oscillator strengths connecting the conduction band electrons with higher

states are spread over at least 28 eV, equation (37) should be applicable for

photon energies between 2.2 and 30.8 eV.

As noted above, the threshold for the excitation of core electrons is

30.8 eV. The threshold transition is from filled states in the L_3 band

whose wave vector lies just outside the Fermi surface to empty states in

the conduction band. The Fermi surface of sodium is very nearly spherical

so the states contributing to the threshold transition do not have to lie on

a symmetry axis.

The expressions for ϵ_1 and ϵ_2 deduced from the Bohm and Pines

model (32, 33) which includes electron correlation effects have the same form

as the expressions deduced from the one-electron model.

Wood (4) observed that sodium films reflected radiation of wavelengths greater than approximately 2100 Å but transmitted shorter wavelength radiation. Zener (7) showed that this observation could be explained by the classical theory if the conduction electrons were assumed to be undamped, i.e., $\gamma = 0$. Under this assumption equations (22) and (23) become

$$n^2 - k^2 = 1 - \frac{\omega_o^2}{\omega^2} \tag{41}$$

and

$$nk = 0 \quad . \tag{42}$$

Equation (42) requires that either n or k is zero. However n and k are both real numbers. Therefore, equation (41) requires that k = 0 for $\omega > \omega_o$ while n = 0 for $\omega < \omega_o$. For k = 0 equation (1) becomes the equation of an undamped wave moving through a medium of index of refraction n. The normal incidence reflectance, R, of radiation incident on a material from vacuum is (29)

$$R = \frac{(n-1)^2 + k^2}{(n+1)^2 + k^2} \quad , \tag{43}$$

so when n = 0, R = 1. That is, all incident radiation is reflected.

Similar conclusions can be reached for both the classical and quantum theories if instead of assuming no damping, it is assumed that the damping, and thus ϵ_2, is small. Equations (14) and (15) can be solved for n and k in terms of ϵ_1 and ϵ_2 giving

$$2n^2 = \epsilon_1 + (\epsilon_1^2 + \epsilon_2^2)^{\frac{1}{2}} \tag{44}$$

and

$$2k^2 = -\epsilon_1 + (\epsilon_1^2 + \epsilon_2^2)^{\frac{1}{2}} \quad . \tag{45}$$

The positive sign must be chosen for the second terms in equations (44) and

(45) to insure that n^2 and k^2 be positive since n and k are real numbers.

Since ϵ_2 is small, the second terms in equations (44) and (45) can be expanded

by the binomial theorem to give

$$2n^2 \doteq \epsilon_1 \pm (\epsilon_1 + \epsilon_2^2/2\epsilon_1) \tag{46}$$

and

$$2k^2 \doteq -\epsilon_1 \pm (\epsilon_1 + \epsilon_2^2/2\epsilon_1) \tag{47}$$

where higher order terms have been dropped. The plus and minus signs in

equations (46) and (47) arise from the square root of ϵ_1^2. Since n and k are

real numbers, n^2 and k^2 are positive. Thus when $\epsilon_1 > 0$, the plus sign must

be chosen in both equation (46) and (47), while if $\epsilon_1 < 0$, the minus sign applies.

That is, when $\epsilon_1 > 0$,

$$n^2 \doteq \epsilon_1 + \frac{\epsilon_2^2}{4\epsilon_1} \tag{48}$$

and

$$k^2 \doteq \frac{\epsilon_2^2}{4\epsilon_1} \tag{49}$$

while when $\epsilon_1 < 0$

$$n^2 \doteq -\frac{\epsilon_2^2}{4\epsilon_1} \tag{50}$$

and
$$k^2 \doteq -\epsilon_1 - \frac{\epsilon_2^2}{4\epsilon_1} \quad . \tag{51}$$

Thus for $\epsilon_1 > 0$ the wave is slightly damped while for $\epsilon_1 < 0$ reflectance is slightly less than 100%. However, the basic features of Zener's theory are unchanged. In the classical theory ϵ_1 is given by equation (22) and the transition from transparency to high reflectivity occurs for $\omega = \omega_o$. In the more general theory ϵ_1 is given by equation (37) and the transition from transparency to high reflectivity occurs for

$$\omega^2 = \frac{\omega_b^2}{1 + 4\pi n \alpha_1} \quad . \tag{52}$$

Energetic electrons passing through a solid can excite collective oscillations of the electrons of the solid if for some frequency, ω_p, $\epsilon^*(\omega_p) = 0$ (35). The collective oscillations are called volume plasmons and their energy is equal to $\hbar \omega_p$ in cubic solids where the transverse and longitudinal dielectric constants are equal. The exciting electron will lose energy equal to $\hbar \omega_p$ times the number of volume plasmons it creates.

If ϵ_2 is non-zero, but small, plasmons will still be formed and will eventually decay giving their energy to either phonons, photons, or electrons. If the damping term, ϵ_2, is small the plasma frequency, ω_p, is to a good approximation the frequency at which $\epsilon_1 = 0$. Thus from equation (37)

$$\omega_p^2 = \frac{\omega_b^2}{1 + 4\pi n \alpha_1} \quad . \tag{53}$$

Comparison of equations (52) and (53) shows that ω_p is the frequency

separating the high frequency spectral region in which the material is

transparent from the low frequency region in which it reflects almost all

incident radiation.

Reflectance and Transmittance at Non-Normal Incidence

The electric intensities of radiation reflected from and transmitted

across the interference between two media are related to the electric

intensity of the incident radiation by Fresnel coefficients r_p, r_s, t_p, t_s. If

E_p^r is the electric intensity of the parallel-polarized component of the

reflected radiation and E_p^o is the electric intensity of the parallel-polarized

component of the incident radiation, then

$$r_p = \frac{E_p^r}{E_p^o} \quad . \qquad (54)$$

Similar equations define the reflection coefficient for perpendicularly

polarized radiation, r_s, and the transmission coefficients t_p and t_s. The

Fresnel coefficients expressed in terms of the angle of incidence, θ_1, the

angle of refraction, θ_2, and the complex indices of refraction of the incident

and refracting media, n_1^* and n_2^*, respectively, are (36):

$$r_p = \frac{n_1^* \cos \theta_2 - n_2^* \cos \theta_1}{n_1^* \cos \theta_2 + n_2^* \cos \theta_1} \quad , \qquad (55)$$

$$r_s = \frac{n_1^* \cos \theta_1 - n_2^* \cos \theta_2}{n_1^* \cos \theta_1 + n_2^* \cos \theta_2} \quad , \tag{56}$$

$$t_p = \frac{2 n_1^* \cos \theta_1}{n_1^* \cos \theta_2 + n_2^* \cos \theta_1} \quad , \tag{57}$$

and

$$t_s = \frac{2 n_1^* \cos \theta_1}{n_1^* \cos \theta_1 + n_2^* \cos \theta_2} \quad . \tag{58}$$

The parameters n_1^*, n_2^*, θ_1, and θ_2 are related by Snell's law,

$$n_1^* \sin \theta_1 = n_2^* \sin \theta_2 \quad . \tag{59}$$

Both θ_1 and θ_2 may be complex.

Since n_1^*, θ_1, n_2^*, and θ_2 can be complex numbers, the Fresnel coefficients are complex numbers and, as such, can be written

$$r_p = |r_p| e^{i\phi_p^r} \quad , \tag{60}$$

$$r_s = |r_s| e^{i\phi_s^r} \quad , \tag{61}$$

$$t_p = |t_p| e^{i\phi_p^t} \quad , \tag{62}$$

and

$$t_s = |t_s| e^{i\phi_s^t} \quad . \tag{63}$$

The advantage of expressing the Fresnel coefficients in this form is shown by

substituting r_p given by (60) into equation (54) giving

$$E_p^r = |r_p| e^{i\phi_p^r} E_p^o \quad . \tag{64}$$

Equation (64) shows that the amplitude of the reflected radiation is $|r_p|$ times the amplitude of the incident radiation and the phase of the reflected radiation is increased by ϕ_p^r relative to the phase of the incident radiation.

CHAPTER III

APPARATUS

General Description

The apparatus, shown schematically in Fig. 2, consisted of a source
of vacuum-ultraviolet radiation, a monochromator to isolate a single wave-
length, and a chamber in which sodium films were formed by thermal
evaporation and their reflectance measured as a function of angle of
incidence. The apparatus had to be evacuated for operation in the vacuum-
ultraviolet and could not contain windows since no window material is
available for radiation of wavelength less than 1050 Å. Vacuum-ultraviolet
radiation was produced by a high voltage gas discharge. Since the radiation
source had to be maintained at a pressure greater than .1 Torr, a differential
pumping assembly between the source and the monochromator, and pumping
systems attached to both the monochromator and the reflectance chamber
were required to maintain proper pressure.

Radiation Source

The source of ultraviolet radiation was a McPherson model 630
capillary discharge tube. The capillary was filled with nitrogen, hydrogen,
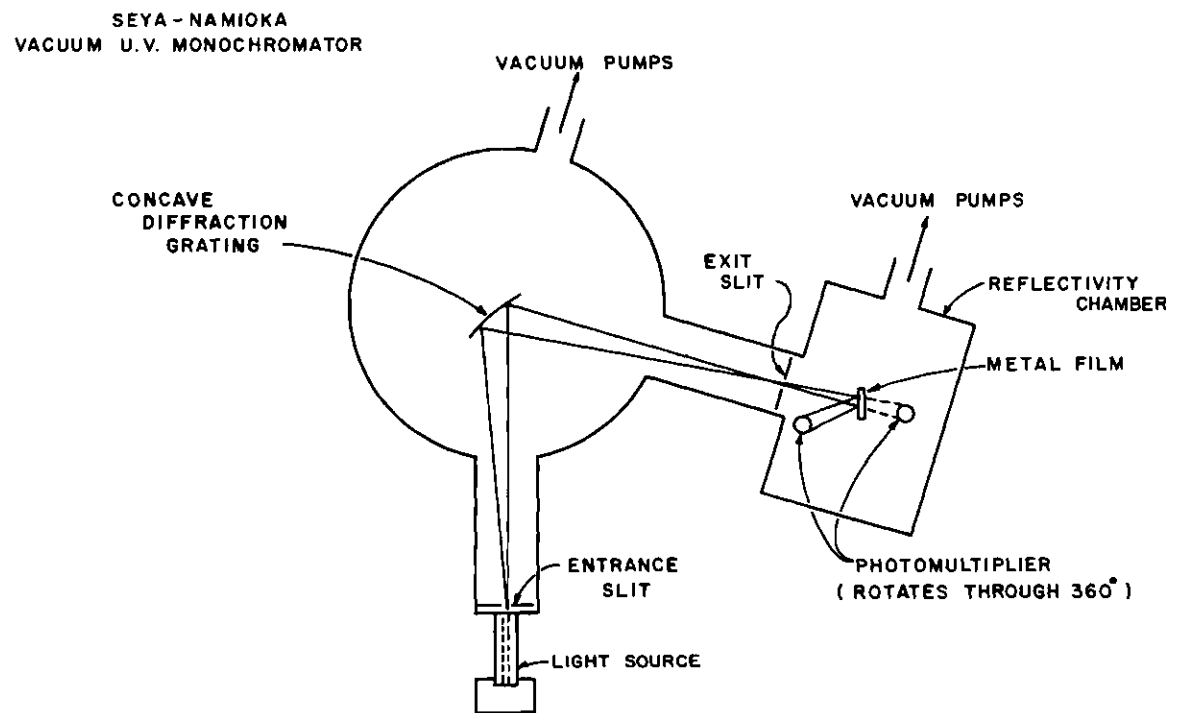air, or other gas, at a pressure between .1 and 1 Torr.

Figure 2. Schematic Diagram of Apparatus

Both circulating water and a fan cooled the glass discharge tube. Two modes

of operation were used to produce vacuum-ultraviolet radiation.

For wavelengths greater than 1000 Å, the discharge tube was connected

directly to a Consolidated Vacuum Corporation, (C.V.C.), model LC031

direct current power supply. In this direct current (dc) mode of operation

the discharge current was about 350 milliamperes.

For wavelengths less than 1000 Å the tube was operated as a con-

densed discharge by connecting the apparatus shown schematically in

Fig. 3 between the dc power supply and the discharge tube. The 2 μfd

capacitor and 8 KΩ resistor reduced the peak current demand on the high

impedance power supply during the charging and discharging of the .4 μfd

capacitor to the discharge tube. For most of the duty cycle the gap was

open and the dc power supply charged the capacitor. When the tungsten rod

in the spark-gap rotor was aligned with the two tungsten poles, sparks

jumped both gaps and the capacitor discharged through the discharge tube.

The discharge, with a peak current of several thousand amperes and a

duration of a few microseconds, caused multiple ionization of the gas atoms

in the discharge tube. The dc power supply operated at about 5000 volts and

150 milliamperes; a repetition rate of 50 discharges per second insured

complete charging of the .4 μfd capacitor. The spark gaps could be adjusted

to compensate for wear by moving the poles.

The intensity of individual spectral lines, measured by the phototube
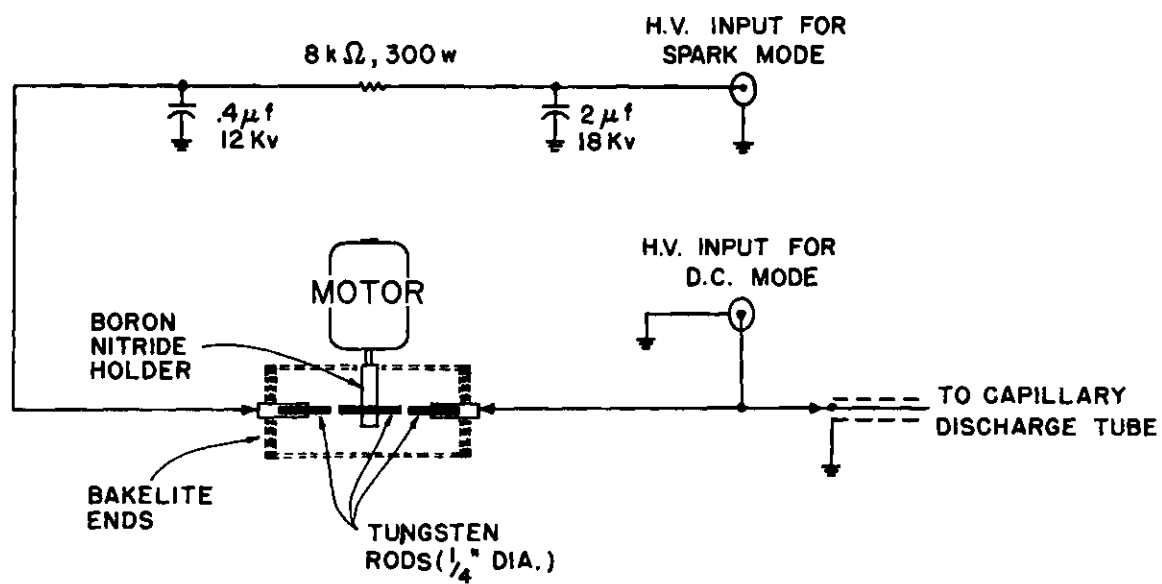
Figure 3. Schematic Diagram of Condensed Discharge Circuit

in the reflectance chamber, was stable within a few percent during the time required for a reflectance measurement. The noise observed in these lines was comparable to the noise observed with the dc mode of operation.

A mercury discharge bulb which produced lines as short as 1849 Å could be installed in place of the discharge tube.

Monochromator

Radiation passed from the discharge tube into a McPherson model 235 vacuum-ultraviolet monochromator of the Seya-Namioka type. Inside the monochromator, the radiation was dispersed by a Bausch and Lomb platinum-coated replica diffraction grating. The grating had a radius of curvature of .5 meters, was ruled with 1200 lines per millimeter, and was blazed for 700 Å.

The exit arm of the monochromator contained a slit whose width was adjustable from 10 to 2000 microns. For normal operation the exit slit was opened to 300 microns. Since the dispersion of the grating was about 13 Å/mm, the resolution of the system was 4 Å.

The exit arm of the monochromator also contained filters of glass, quartz, and lithium fluoride which could be inserted into the path of radiation leaving the monochromator. The filters were used to distinguish between first and second order reflections and also to help determine the intensity of background radiation.

Reflectance Chamber

The reflectance chamber, a stainless steel cube 10 inches on a side, was connected directly to the exit arm of the monochromator. A sodium film was formed on a quartz substrate inside the chamber by high-current thermal evaporation from a tantalum boat. The substrate was mounted on a sample holder which could be rotated to vary the angle at which radiation was incident on the film as shown in Fig. 4. The holder could also be raised to permit measurement of the intensity of the incident radiation. The intensities of the incident and reflected beams were measured with an RCA 1P21 photomultiplier coated with sodium salicylate. The photomultiplier was operated at 600 volts from an Atomic Instrument Co. model 312 high voltage power supply. The photocurrent was measured by a Keithley model 409 picoammeter and recorded on a Brown chart recorder. Photocurrents ranged from 10^{-7} to 10^{-10} amperes. A cold finger in the chamber was filled with liquid nitrogen to provide cryogenic pumping during evaporation. The evaporation equipment, sample holder, photomultiplier, and cold finger were mounted on stainless-steel flanges which were sealed to this chamber by Viton O-rings.

Angle Doubler

The photomultiplier and sample holder were connected by an angle-doubling mechanism so that the phototube was rotated through twice the angle of the sample and remained in the reflected beam. The angle-doubling

CIRCULAR SCALE

SPLIT TYPE
CLUTCH HUB

VACUUM
CHAMBER

SYNC. GEAR
MOTOR

PHOTOMULTIPLIER
TUBE

SAMPLE
HOLDER

WORM GEAR
DRIVE

"NO-SLIP"GEAR PULLEY
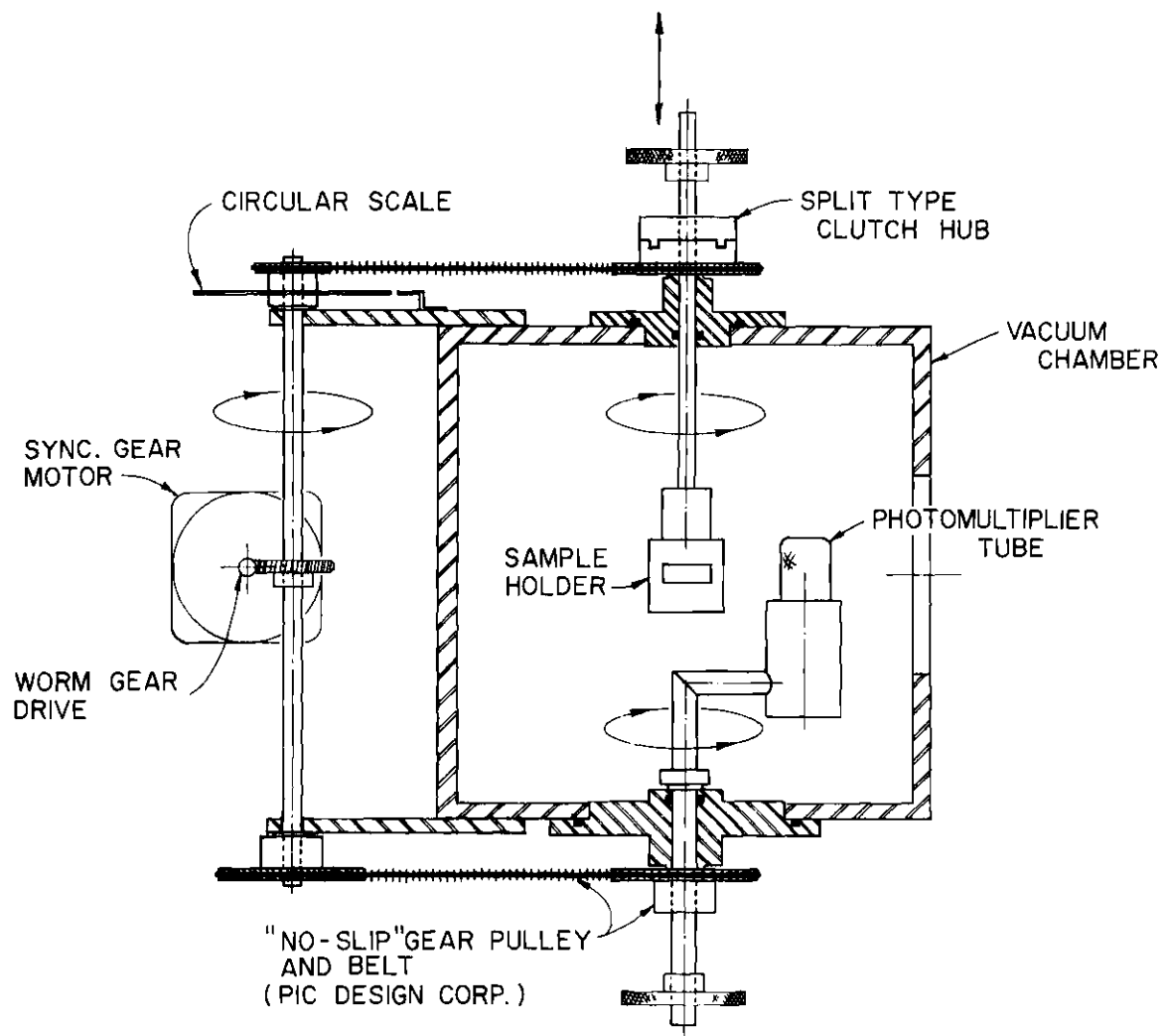AND BELT
(PIC DESIGN CORP.)

Figure 4. Schematic Diagram of Reflectance Chamber and Angle Doubler

mechanism is shown schematically in Fig. 4. The shafts which support the

photomultiplier and sample holder are connected to an external shaft by

toothed nylon belts and associated toothed pullies supplied by Precision

Instruments Corporation. The shaft of the sample holder was connected

to its pulley by a split type clutch hub to facilitate withdrawal of the

sample from the beam. The external shaft was driven by a five-speed

synchronous motor. The angle, θ, at which radiation was incident on the

sample was read within $\pm$ .25° from a vernier scale mounted on the exterior

shaft. The speeds of the synchronous motor were chosen so that the

divisions on the chart paper represented convenient multiples of degrees.

The design of the angle doubler had two important advantages. First,

there was no appreciable backlash in the assembly. Second, all of the

components of the angle doubler were outside the vacuum system so adjust-

ments could be made without breaking the vacuum.

Hemi-Cylinder

Sodium is extremely reactive and thus the surface of a freshly-formed

film was covered with a thin layer of oxide within a few seconds after

evaporation even though the pressure in the reflectance chamber was less

than 10^{-6} Torr. While the reflectance of the oxidized vacuum-sodium

surface can be used to determine the index of refraction, it is desirable to

be able to measure the reflectance of unoxidized sodium surfaces for two

reasons. First, measurements made on "clean" surfaces verify that the

values of the index of refraction determined from the reflectance of oxidized

surfaces are not influenced by the presence of the oxide. Second, the

extinction coefficient, k, of sodium can be determined from the reflectance

of an unoxidized surface.

The film surface adjacent to the substrate is protected from oxidiza-

tion by the substrate and thus, when viewed through the substrate, is an

uncontaminated sodium surface. If the film had been deposited on a parallel-

sided substrate, reflection and refraction effects and absorption of

radiation by the substrate would have complicated the determination of the

reflectance of the sodium surface. However, these difficulties were over-

come by evaporating the sodium onto a quartz hemi-cylinder as shown in Fig.

5. Radiation entered and left the hemi-cylinder normal to its curved

surface so that the angle of incidence at the quartz-vacuum surface was not

affected. Further, the intensity lost by reflection when the radiation

entered and left the hemi-cylinder, and by absorption during its passage

through the hemi-cylinder was independent of the angle of incidence. One of

the hemi-cylinders used in this work was made of suprasil grade quartz* and

was transparent to radiation of wavelength greater than 1700 Å.

Typical reflectance measurements made through the hemi-cylinder

are shown in Fig. 6. The lower portion of the figure shows the recorder

tracing of the reflectance of 1849 Å radiation from a sodium film. The film

_____

*Hemi-cylinder supplied by Amersil Quartz Division, Engelhard Industries,
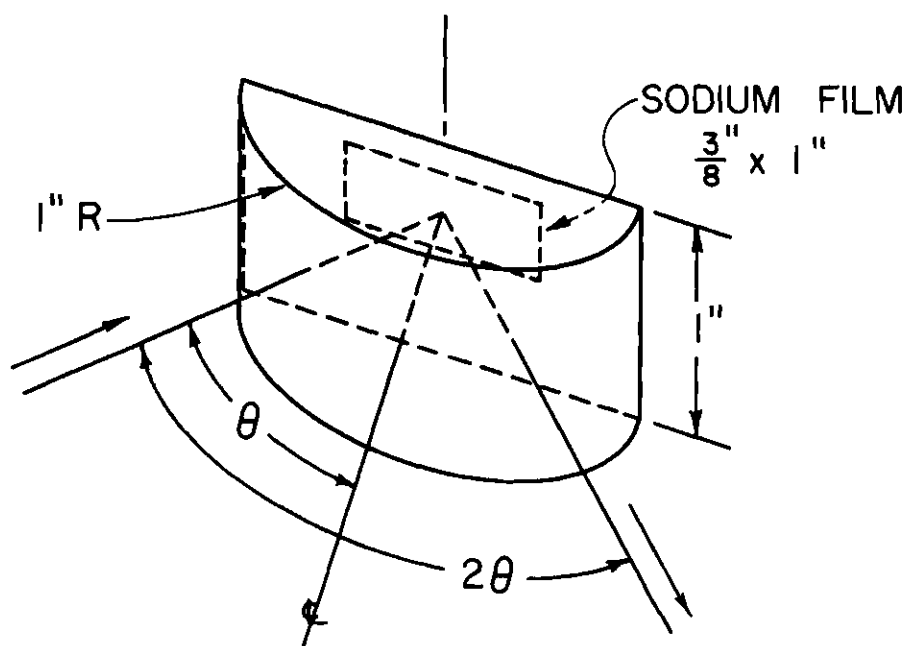Inc., Hillside, New Jersey.
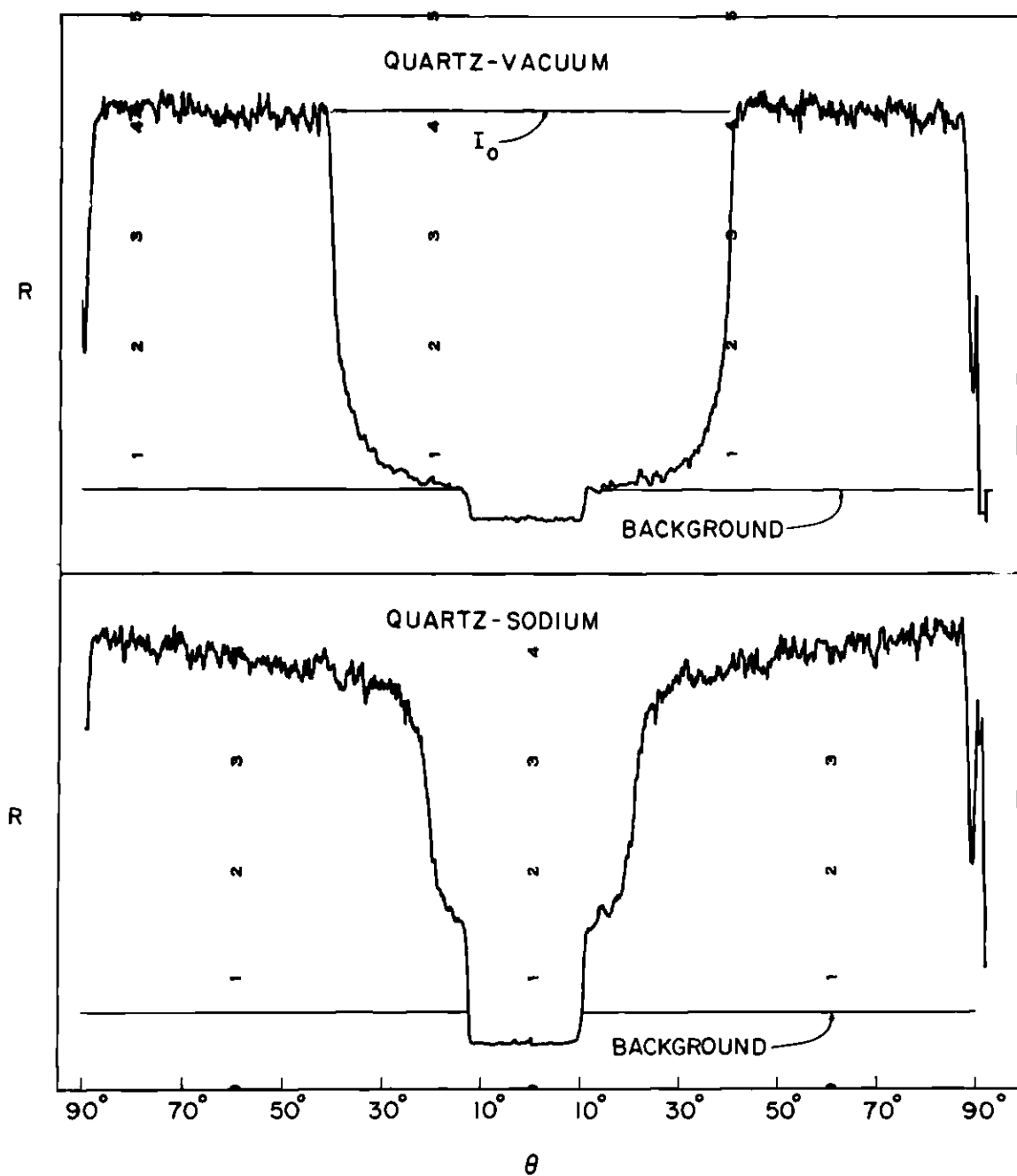
Figure 5. Diagram of Hemi-Cylinder

Figure 6. Reflectance of 1849 Å Radiation from a Quartz-Vacuum and a Quartz-Sodium Interface Measured as a Function of Angle of Incidence

was made very thick (about 20,000 Å) so that interference fringes were not observed. The recorder tracing shown in the upper portion of Fig. 6 was made by raising the hemi-cylinder one-half inch so that the incident radiation was reflected from the quartz-vacuum interface. The hemi-cylinder was raised by inserting a spacer in the split clutch hub. The reflectance of the quartz-vacuum interface is used to determine the index of refraction of the hemi-cylinder and to determine the intensity of the incident radiation, I_o.

Vacuum System

The apparatus was evacuated by pumps connected to the reflectance chamber, the monochromator, and a differential-pumping assembly located between the capillary-discharge tube and the monochromator. A National Research Corporation six-inch oil diffusion pump backed by a Welch 1397 rotary forepump was connected to the reflectance chamber via a water-cooled baffle and a gate valve. The monochromator was evacuated by a C.V.C. four-inch oil-diffusion pump backed by an Edwards Speedivac 250 rotary forepump and separated from the monochromator by a water-cooled chevron-baffle and a gate valve. The high pressure side of the McPherson differential pumping assembly was connected directly to a Cenco Hyvac 45 rotary fore-pump, while the low pressure side was connected to a pumping system identical to the one attached to the monochromator.

Pressure in the system was monitored by a C.V.C. ionization gauge connected to the reflectance chamber. Pumping for twelve hours reduced the pressure in the reflectance chamber to about 1×10^{-6} Torr. Addition of liquid nitrogen to the cold finger reduced the pressure in the chamber to less than 3×10^{-7} Torr. Evaporation caused a pressure surge to between 5×10^{-6} and 1×10^{-5} Torr.

CHAPTER IV

EXPERIMENTAL PROCEDURE

Alignment of the Optical System

The wavelength selected by the monochromator was read from a digital

scale. For the grating used in this work two scale divisions were equal to

one Angstrom. The scale reading corresponding to a wavelength of zero

Angstroms was determined by observing the location on the scale of the

maximum intensity of radiation reflected specularly from the grating (i. e.,

the central image). The calibration of the monochromator scale was checked

for linearity by comparing the scale readings of prominent spectral lines

(e.g., the Lyman α line in the hydrogen dc spectrum) with the accepted

values of their wavelengths (37, 38).

The alignment of the sample holder and vernier scale required the

replacement of the capillary discharge tube by a tungsten light bulb. The

grating of the monochromator was then set to the central image (λ = 0) so

that a collimated beam of white light passed through the exit slit of the

monochromator and into the reflectance chamber. A ground glass plate

replaced the hemi-cylinder in the sample holder so that the beam of light

from the monochromator produced an easily-visible rectangular illuminated

area. The illuminated area was approximately 3 millimeters high and 2

millimeters wide for normal incidence. The same area was covered by ultra-violet radiation since the exit slit of the monochromator was opened to 300 microns for both reflectance measurements and alignment. The flange which held the sample holder was adjusted until the axis of the sample holder inter-sected the axis of the beam emerging from the monochromator. The align-ment was considered satisfactory when the illuminated area increased in width symmetrically as the sample holder was rotated clockwise or counter-clockwise from normal incidence. When satisfactory alignment had been obtained, the flange on which the sample holder was mounted was bolted securely in place. The alignment of the sample holder was then rechecked.

The angle at which radiation was incident on the sample was read from a circular scale calibrated in degrees and mounted on the external shaft of the angle doubler as shown in Fig. 4. A plate on which an index and a vernier scale were marked was bolted to the frame of the angle doubler next to the edge of the circular scale. The scale was calibrated by placing an aluminum mirror in the sample holder and adjusting the sample holder to near normal incidence. The circular scale was adjusted until the zero mark was opposite the index mark on the plate. The set screw was then tightened. Fine adjustment was accomplished by turning the sample holder until the beam reflected from the mirror passed back through the exit slit of the monochromator. The light which passed back into the monochromator was observed by removing the plate which covered the top of

the monochromator and placing a glass slide in the beam leaving the grating

at an angle of 45° with respect to the beam. The monochromator side of the

exit slit was viewed as a reflected image. When the plane of the sample

holder was perpendicular to the incident beam the exit slit was filled with

light which had passed through the slide and through the exit slit and had

then been reflected by the mirror back through the exit slit. If the zero

mark on the circular scale was no longer opposite the index mark, the bolts

which held the index plate were loosened and the position of the plate ad-

justed. The calibration of the circular scale was checked again after the

mirror had been replaced by the hemi-cylinder. The angle of incidence read

from the circular scale was accurate within $\pm$ 1/4 degree.

Preparation of Sodium Films

Sodium films were prepared in the evacuated reflectance chamber by

thermal evaporation from a tantalum boat. The boat, a cylinder with closed

ends and a hole in one side, was heated by passing a current through it.

Vaporized sodium atoms escaped through the hole and were condensed on the

flat surface of the quartz hemi-cylinder which was described in Chapter III.

Prior to being mounted in the sample holder, the hemi-cylinder was cleaned

with detergent, lens paper, and a chromic acid bath.

Before evaporation, the sodium was degassed by gently warming the

boat. While the degassing was in progress a shutter protected the substrate.

The shutter was mounted on a shaft which passed through an O-ring seal in

the side of the reflectance chamber. Thus the shutter could be rotated

from outside the chamber. After the sodium had been degassed for 10 to

20 minutes, the current through the boat was increased to melt the sodium

and start evaporation. When rapid evaporation had begun, the shutter,

which protected the substrate was opened for a few seconds. Films between

4000 Å and 5000 Å thick, the range of thicknesses which gave the best

interference patterns, were formed by exposing the substrate for from two

to five seconds. Twenty second exposures yielded films in excess of

20,000 Å thick film. The vacuum side of the thick films was rougher than

the vacuum side of films 4000 to 5000 Å thick. However, the reflectance

measured from the quartz side of the thick films was not complicated by

interference effects.

Pressure in the reflectance chamber was strongly influenced by the

temperature of the tantalum boat. When the cold finger was filled with

liquid nitrogen and the capillary discharge tube was in operation but the boat

was not being heated, the pressure in the reflectance chamber was approxi-

mately 3×10^{-7} Torr. Heating the boat to degas the sodium caused an

increase in pressure. After the initial surge, the pressure stabilized at

1 or 2×10^{-6} Torr. When the current through the boat was raised to

evaporate the sodium, pressure in the chamber increased to between 5×10^{-6}

and 2×10^{-5} Torr. The pressure returned to 10^{-6} Torr in a few seconds

after evaporation ceased, and to the mid 10^{-7} range within 5 to 10 minutes.

During the evaporation, the photomultiplier and the curved portion of the hemi-cylinder were protected by teflon tape or aluminum foil masks to prevent them from being coated with sodium. The covers were removed after evaporation was complete.

The purity of the sodium exceeded 99.5%. Spectro-chemical analysis* of a bulk sodium sample revealed: .34% potassium, .001% calcium, .005% lithium, less than .0001% rubidium, and less than .0002% cesium. When the boat was being placed in the reflectance chamber prior to an evaporation, the sodium was exposed to air for about a minute and became covered with a layer of oxide. However, the oxide was much less volatile than metallic sodium and remained in the boat when the evaporation was performed.

Reflectance Measurements

The procedures followed before and after evaporation were designed to minimize the interval between formation of the film and the first reflectance measurement. To insure stable operation of the capillary discharge, the pressure in the dischrage tube had to be carefully adjusted and the tube given an opportunity to warm up. Therefore, the discharge was turned on and adjusted before the evaporation. Also, the wavelength scale of the monochromator was set to an intense line before the evaporation. After the evaporation was complete, the shutter which protected the

*Analysis performed by the Analytical Chemistry Division, Oak Ridge National Laboratory.

substrate was moved to the side of the reflectance chamber, the covers were removed from the phototube and the curved portion of the hemi-cylinder, light-tight covers were placed over the observation ports in the evaporation flange, the photomultiplier was energized, and the chamber was checked for light leaks by turning off the lights in the room, while monitoring the photomultiplier output current. The minimum time between evaporation and the start of the reflectance measurements was five minutes.

All reflectance measurements were made for one wavelength at a time rather than by scanning over the spectrum. The maximum intensity of each line was obtained by manually adjusting the wavelength scale of the monochromator while observing the output of the photomultiplier. The motor-driven angle doubler was used to measure reflectance as a function of angle of incidence. Figures 7 and 8 show the reflectance of 1580 Å and 836 Å radiation, respectively, from a sodium film exactly as it was recorded on chart paper. The speed of the angle doubler was such that the smallest division on the chart paper represents an angle of 2° in Fig. 7 and 1° in Fig. 8. Other speeds were also used. For measurements made from the vacuum side of the sodium, the reflectance scale was calibrated by with-drawing the sample and measuring the intensity of the incident radiation with the phototube. The calibration of the circular scale was not affected when the sample holder was raised since the sample-holder shaft was connected to the angle-doubler pulley by a split clutch hub. The photo-
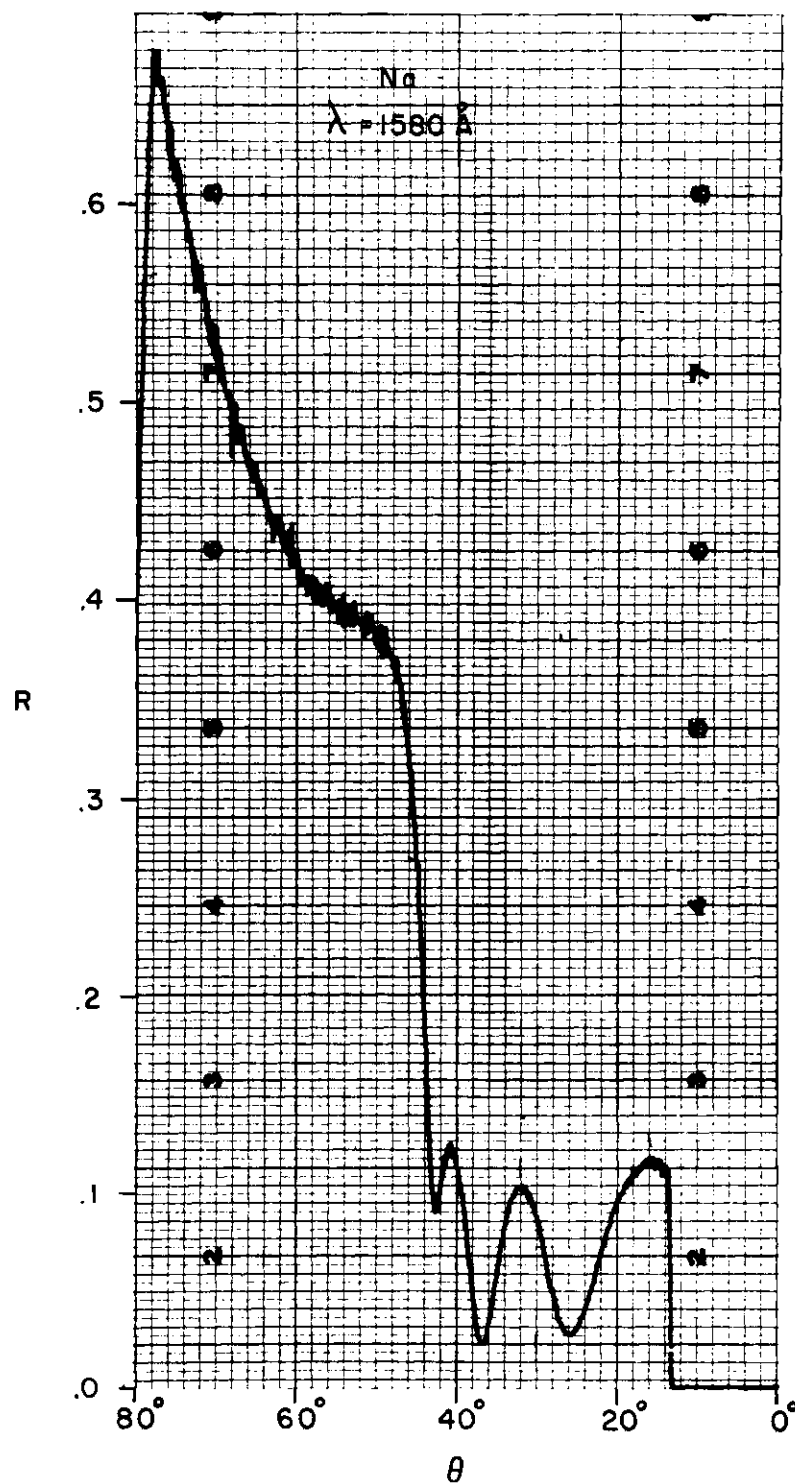
Figure 7. Chart Recorder Plot of Reflectance of 1580 Å Radiation from a
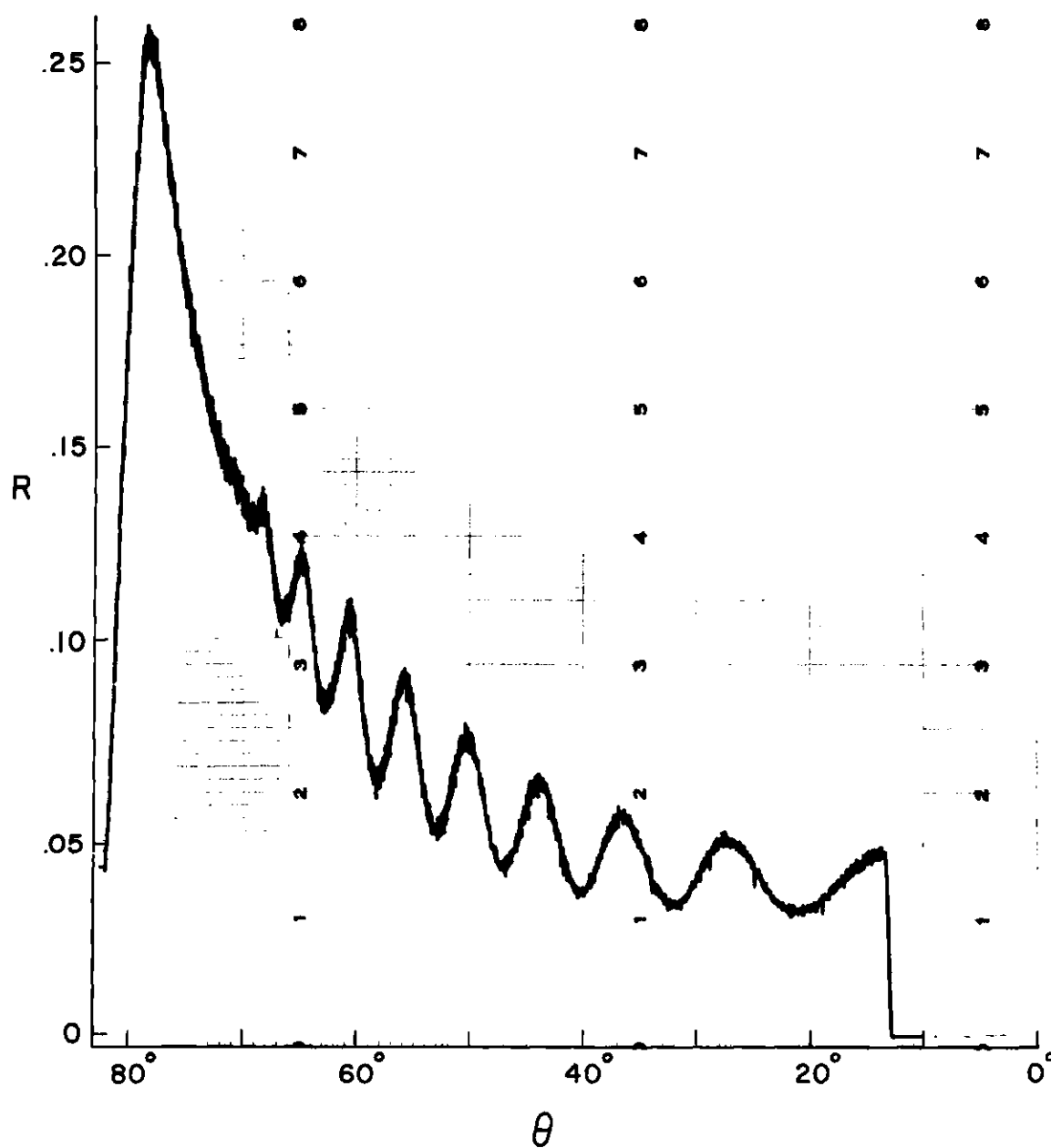Sodium Film as a Function of Angle of Incidence

Figure 8. Chart Recorder Plot of Reflectance of 836 Å Radiation from a
Sodium Film as a Function of Angle of Incidence

multiplier blocked the incident radiation for angles of incidence less than

about 13°, while for angles greater than 78°, the sample holder obstructed

the beam. The significance of the structure in the reflected radiation for

angles between 13° and 78° will be discussed in Chapter V.

For measurements made from the quartz side of the sodium film

(i.e., through the hemi-cylinder) the reflectance scale was calibrated by

comparing the reflectance of the quartz-vacuum interface with the

reflectance of the quartz-sodium interface. The reflectance of 1746 Å

radiation from these two interfaces is shown in Fig. 6. For angles of

incidence greater than the critical angle of the quartz-vacuum interface

(40° in Fig. 6), total reflection occurs. Thus the reflectance measured

in this region determines the intensity of the incident radiation I_o. This

intensity is used to calculate the reflectance $R(\theta)$ of the quartz-sodium

surface from the equation

$$R = \frac{I(\theta)}{I_o} \tag{65}$$

where $I(\theta)$ is the intensity of the radiation reflected from the quartz-

sodium interface. Equation (65) gives R since the fraction of the radiation

lost by reflection when the radiation entered and left the hemi-cylinder and

by absorption while passing through the hemi-cylinder (about 20% for 1849 Å)

was the same in the two cases.

Determination of Background

Before reflectance could be determined for a given wavelength it was necessary to know what portion of the photomultiplier's output was due to radiation of the desired wavelength and what portion was due to scattered radiation of other wavelengths and to the dark current of the photomultiplier. The combined contributions of the latter two effects are called the background of the system. For the diffraction grating used in this work the background was independent of the wavelength setting of the monochromator for wavelengths greater than 500 Å. For wavelengths less than 500 Å the background increased as the central image was approached. Thus when operating the capillary tube in the dc mode, the background was determined by observing the response of the photomultiplier when the wavelength scale of the monochromator was set to 800 Å, since a dc discharge in hydrogen or nitrogen produces no radiation of wavelength less than 900 Å. The condensed-discharge mode of operation of the capillary tube was characterized by well-separated spectral lines and the background was determined by selection of a wavelength setting between two lines which gave a minimum response of the photomultiplier. The background was measured separately for the incident radiation, I_o, and for each $I(\theta)$ of interest. Then the background reading was subtracted from the direct reading to determine the portion of the measured intensity which was not caused by the background.

The background correction introduced negligible uncertainty in

reflectances measured for strong spectral lines. However, errors as large as 2 or 3% could be expected in reflectances measured with very weak lines.

An alternate method was used to locate the background for measurements made on quartz-sodium surfaces. This method depended on the fact that when k is small, reflectances for angles less than the critical angle depend to a good approximation only on the index of refraction of the reflecting surface and the polarization of the incident radiation. The index of refraction was known from the location of the critical angle. The reflectance for an angle of incidence of 14°, calculated from the index of refraction and the previously determined polarization of the incident radiation (45), was compared with the reflectance measured at this angle to obtain the background.

CHAPTER V

DETERMINATION OF OPTICAL CONSTANTS

Introduction

The methods commonly used for the determination of the optical

constants of materials in the vacuum ultraviolet region require either

measurement of the reflectance at two angles of incidence for each photon

energy or measurement of reflectance at normal incidence for all photon

energies. In the first method, which is usually described as the "two

angle method", the optical constants n and k (or ϵ_1 and ϵ_2) are found for

each wavelength from the two reflectances measured at that wavelength

(39,40). In the second method, a Kramers-Kronig analysis (41) is performed,

and the optical constants for one photon energy are determined by the

reflectances measured for all photon energies. However, the two-angle

and Kramers-Kronig methods are difficult to use on sodium. Because it

is highly reactive, the surface of a sodium film exposed to a vacuum of 10^{-6}

Torr is covered with oxide* in a few seconds after it is formed and the oxide,

which absorbs strongly in the vacuum-ultraviolet wavelength region, changes

---

*The surface layer is referred to as "oxide" for convenience. The chemical
composition of the layer was not investigated.

the reflectance of the surface. This difficulty was overcome by both the
critical-angle method and interference methods, both of which gave values
of the index of refraction.

In addition, use of the quartz hemi-cylinder described in chapter III
made possible the measurement of the reflectance of uncontaminated
sodium surfaces in part of the spectral region of interest. These measure-
ments served as a check on the values of n given by the critical angle and
interference measurements made on the exposed surface of the sodium and
also made possible the determination of the extinction coefficient, k.

Critical-Angle Method

The critical-angle method can be used to determine the index of
refraction, n, of a material if n is less than 1.0 and the extinction
coefficient, k, of the material is small. For transparent materials (k = 0)
the critical angle, θ_c, marks the start of total reflectance; the slope of
reflectance _versus_ angle of incidence is discontinuous at θ_c. If k is greater
than zero, the discontinuity in the reflectance curve disappears, but if k is
small, there is a rapid increase in reflectance near θ_c. Hunter (42) has
calculated the reflectance, R, as a function of angle of incidence, θ, for
values of n from .1 to .9 and values of k from .001 to .2. The calculations,
which required evaluation of the Fresnel reflection coefficients (equations 55,
56) were made for parallel and perpendicular polarized incident radiation and
also unpolarized incident radiation. Hunter's calculations show that the angle

at which the slope of the reflectance curve is a maximum, θ_m, can be used as

an approximate value of the θ_c. When k is greater than about .05, correction

factors must be applied to θ_m. However, measurements made with the

quartz hemi-cylinder show that for 2000 Å wavelength radiation (the longest

wavelength for which values of n were determined) the extinction coefficient

of sodium is .036 $\pm$ .003. Also, according to equations (22), (23), and (49),

k decreases as λ decreases. Thus for $\lambda \leq 2000$ Å, the correction factors

are not necessary, and the index of refraction is given by

$$n = \sin \theta_m \quad . \tag{66}$$

Figure 9 shows the reflectance, R, of 1580 Å radiation from a sodium film

deposited on a quartz substrate as a function of θ. The angle of maximum

slope, θ_m, is 44° $\pm$ .5°. Thus, at this wavelength the critical angle gives

n = .695 $\pm$ .013. Values of the index of refraction of sodium determined by

the critical angle method for three sodium films are given in Table 1. All

measurements on film A were made from the vacuum side of the film since

this film was deposited on a hemi-cylinder which did not transmit well

below 2000 Å. All measurements on film B were made from the quartz side

of the film since the thickness of this film exceeded 20,000 Å and, as a

result, the vacuum surface was extremely rough. Measurements were made

on both sides of film C.

Oxide which forms on the surface of the sodium which is exposed to

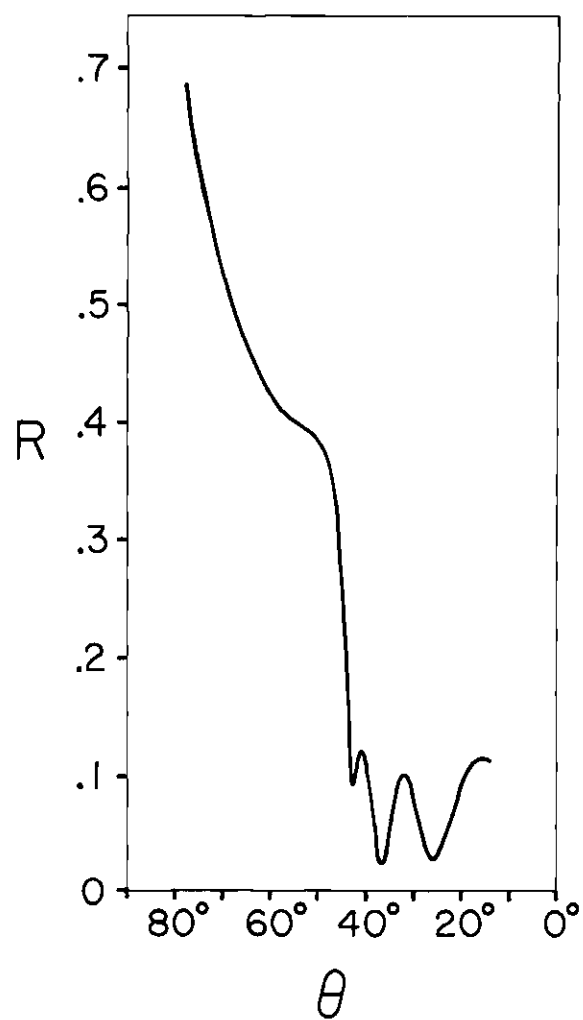vacuum reduces the reflectance for angles of incidence greater than the

Figure 9. Tracing of Reflectance of 1580 Å Radiation Reflected from a Sodium Film as a Function of Angle of Incidence

Table 1

Index of Refraction of Sodium as a Function of Wavelength

λ (Å)	Film A Critical Angle	Film A Interference	Film B Critical Angle	Film C Critical Angle	Film C Interference	n Average	$\epsilon_1 = n^2$
420		1.020				1.020	1.040
437		1.012				1.012	1.023
448		1.011				1.011	1.023
460		1.002				1.002	1.003
486		.993				.993	.986
587		.979				.979	.959
685		.964			.970	.967	.935
765		.949				.949	.901
802		.942				.942	.888
824		.936				.936	.876
836		.935				.935	.873
881		.922				.922	.850
903		.917				.917	.840
924		.914			.919	.916	.839
950	.917	.910				.914	.834
974	.908	.906				.907	.823
1006					.906	.906	.821

Table 1 (Continued)

1048	.891	.884				.887	.788
1085					.885	.885	.783
1119	.870	.871				.870	.758
1189				.854	.849	.852	.726
1216	.844	.842				.843	.711
1277	.820	.817				.819	.671
1356	.798	.802				.800	.640
1436	.760	.764				.762	.581
1493				.737		.737	.543
1547	.707	.715				.711	.506
1580	.695	.704				.700	.490
1635	.670	.680				.675	.455
1692	.640	.642				.641	.404
1716				.626		.626	.392
1722			.622			.622	.387
1739	.616	.616				.616	.380
1743			.618	.608	.615	.611	.373
1754				.602		.602	.362
1786			.583			.583	.340

Table 1 (Continued)

1800	.574	.574	.578	.576	.332
1850	.530	.536	.538	.535	.286
1900	.485		.510	.502	.252
1925			.491	.491	.241
1950	.454		.460	.457	.209
1975			.438	.438	.192
2000	.390		.418	.404	.163

critical angle as can be seen by comparison of the reflectance of sodium

shown in Figure 6, with that shown in Figure 9. Similar reductions in

reflectance of aluminum films have been observed experimentally by Madden,

Canfield and Hass (43). These authors calculated the reflectance of an

aluminum surface covered with a uniform layer of aluminum oxide 10 to 30 Å

thick using the experimentally-determined values of n and k of both aluminum

and aluminum oxide. The reflectance calculated for an oxidized surface

was less than the reflectance calculated for an unoxidized surface in

agreement with the experimental measurements. However, Hunter (42)

found that the angle of maximum slope was not seriously affected by

surface oxide.

Hunter's calculations could not be repeated for a sodium surface

covered with a layer of oxide because the optical constants of the oxide were

not known. However, the critical angles obtained from the reflectance

measurements made through the hemi-cylinder on the unoxidized quartz-

sodium interface gave values of n in good agreement with the values obtained

from the vacuum-sodium interface shown in Table 1. Note that when

measurements are made through the hemi-cylinder, equation (66) must be

changed to

$$n = n_{qz} \sin \theta_m^{qz} \tag{67}$$

where θ_m^{qz} is the angle of maximum slope of R $\underline{vs}$ θ measured through the

hemi-cylinder and n_{qz} is the index of refraction of the quartz. The values of

n_{qz} used in equation (67) were obtained from the critical angle of the quartz-vacuum interface shown in the upper portion of Fig. 6. Table 2 gives values of n_{qz} for λ from 1700 Å to 2000 Å.

Interference Method

Interference fringes which appear in Figs. 9 and 10 at angles of incidence less than the critical angle can also be used to determine the index of refraction of the sodium film. Interference is caused by the difference in phase of components of the incident radiation reflected from the front and rear surfaces of the film. These components are labeled I and II in Fig. 11. The optical paths traveled by components I and II differ by $2T(n^2 - \sin^2 \theta)^{\frac{1}{2}}$, where T is the thickness of the film. In addition, changes in the phase of the components reflected from or transmitted through a surface of the film cause an additional optical path difference of $P\lambda$ where λ is the wavelength of the radiation. Thus the positions of maxima and minima in the interference pattern are given by

$$N\lambda = P\lambda + 2T(n^2 - \sin^2 \theta)^{\frac{1}{2}} \tag{68}$$

where N, the order of interference, is an integer for interference maxima and a half-integer for interference minima. A systematic method of finding the value of N of each interference fringe is to rearrange equation (68) so that it is in the form of an equation of a straight line in the variables $\sin^2 \theta$ and $(N - P)^2$, i.e.

Table 2. Index of Refraction of a Suprasil-Quartz Hemi-Cylinder
As a Function of Wavelength

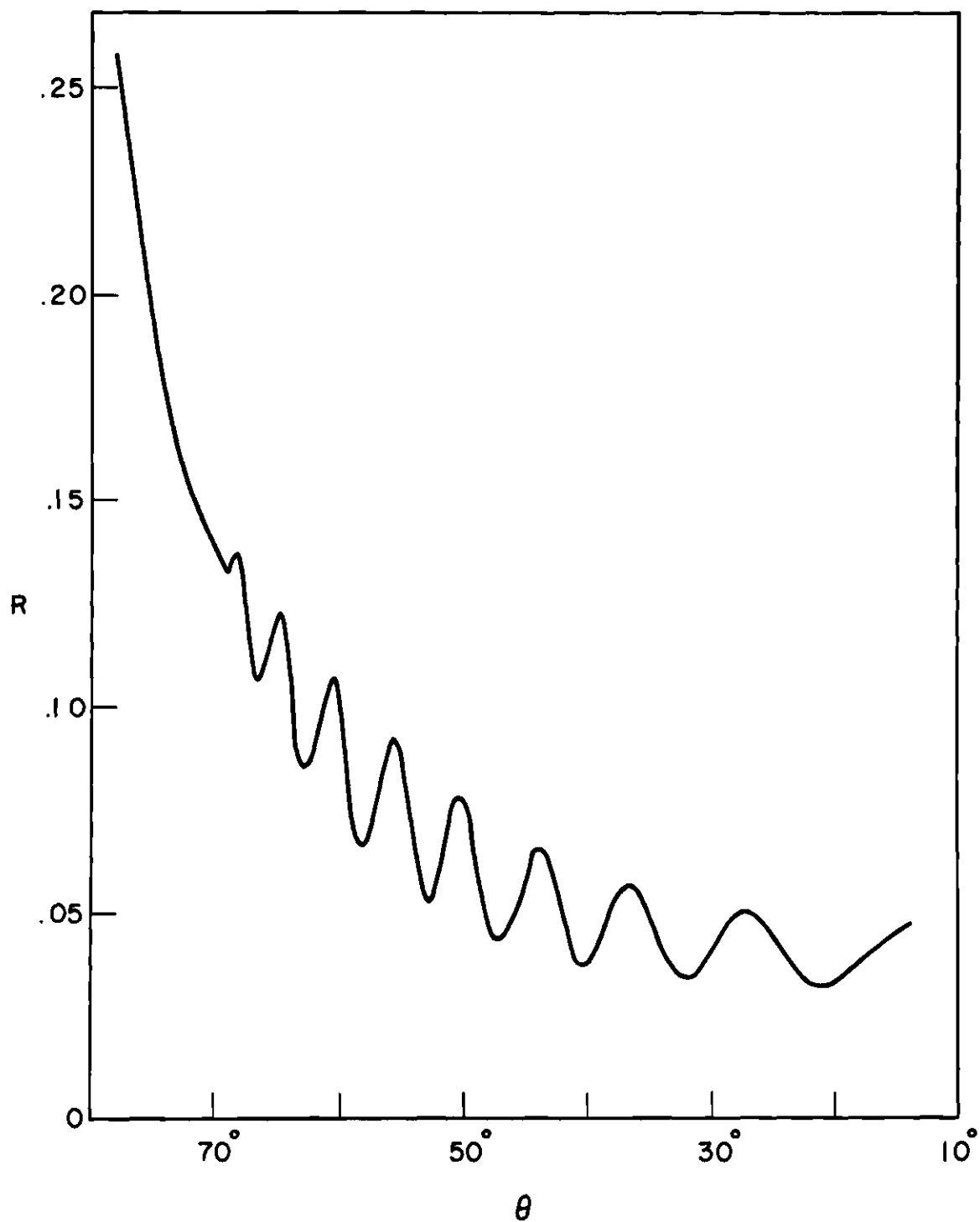| $\lambda\ (\text{Å})$	n
1700	1.565
1750	1.555
1800	1.545
1850	1.537
1900	1.530
1950	1.523
2000	1.515

Figure 10. Tracing of Reflectance of 836 Å Radiation Reflected from a
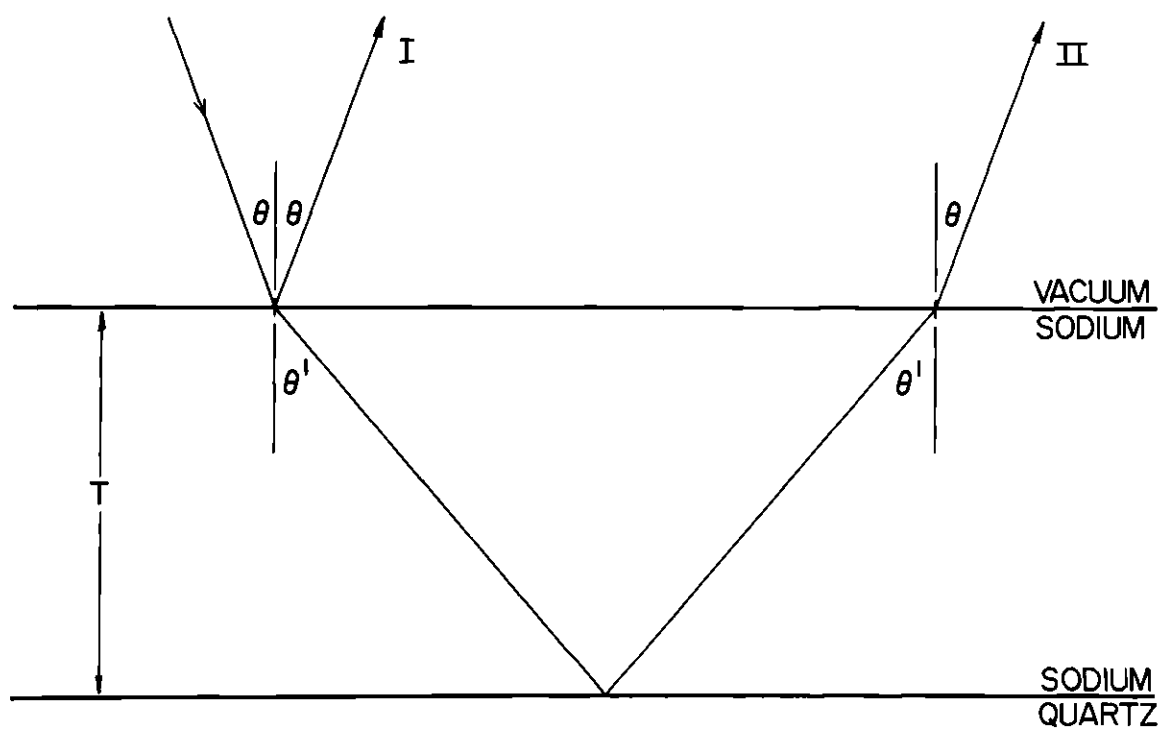Sodium Film as a Function of Angle of Incidence

Figure 11. Cross Section of a Sodium Film on a Quartz Substrate

$$\sin^2 \theta = n^2 - (\lambda/2T)^2(N - P)^2 \quad . \tag{69}$$

The parameter P represents a correction which is equated to zero until the proper values of N have been found.

Different values of N are assigned to the observed maxima and minima with the restriction that the orders of an adjacent maximum and minimum differ by $\frac{1}{2}$. Then a straight line is fit by the method of least squares to the values of $\sin^2 \theta$ and N^2 where θ is the observed angle of incidence of an interference maximum or minimum, and N is the order of interference which has been assigned to that maximum or minimum. Three such lines are shown in Fig. 12. The values of $\sin^2 \theta$ used in this figure are those of the interference pattern of 836 Å radiation shown in Fig. 10. The interference maximum located at 65° in Fig. 10 was assigned an order of 2 in line I of Fig. 12, an order of 3 in line II, and an order of 4 in line III. A function E, equal to the sum of the squares of the differences between the experimental values of $\sin^2 \theta$ and the values of $\sin^2 \theta$ given by the least-square line, was computed for each line. The correct orders of interference are those which give the smallest value of E. In Fig. 12, line II has the smallest values of E. Thus the order of the maximum observed for θ of 65° is 3, the order of the minimum at about 63° is 3.5, and so on.

The quantity P is equal to $-\frac{1}{2\pi}$ times the net phase difference due to reflections and transmissions of components I and II of Fig. 11 in radians.
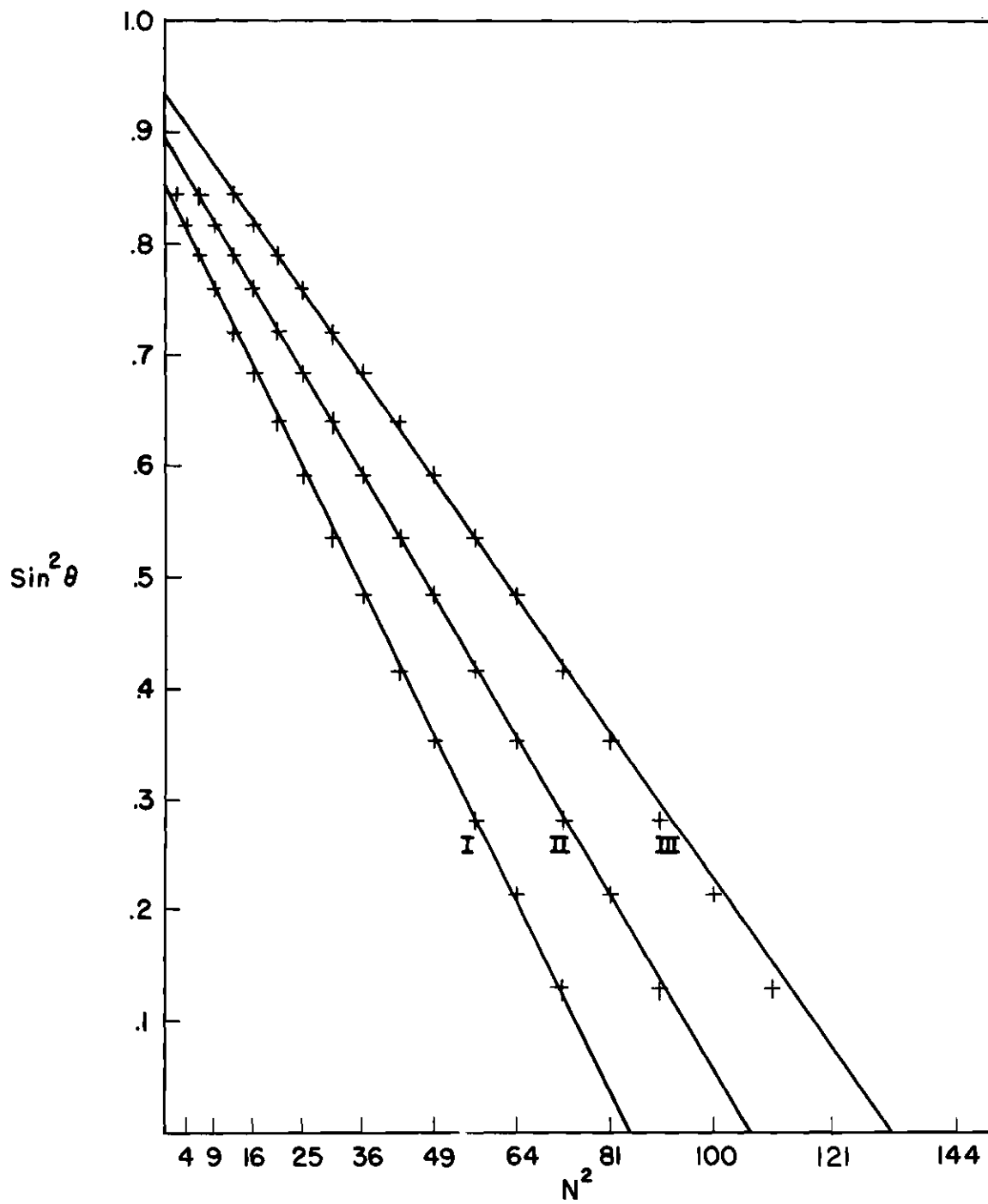
Figure 12. Sin^2 θ Versus N^2 for three sets of order numbers

That is,

$$2\pi P_i = \left[\phi_i^r(\text{vac}, \text{Na}) - \left\{ \phi_i^t(\text{vac}, \text{Na}) + \phi_i^r(\text{Na}, \text{qz}) + \phi_i^t(\text{Na}, \text{vac}) \right\} \right] \qquad (70)$$

where $\phi_i^r(\text{vac}, \text{Na})$ is the argument of the complex Fresnel reflection coefficient of a vacuum-sodium interface, $\phi_i^t(\text{vac}, \text{Na})$ is the argument of the transmission coefficient for that interface, and so on. The subscript i stands for the polarization of the radiation. If both of the media forming an interface are transparent, ϕ_i^r will be either 0 or π radians, while ϕ_i^t is always 0. However, if the extinction coefficient of one or both of the media forming an interface is nonzero, the phase changes caused by reflection and transmission will depend on the angle of incidence, the optical constants (n and k) of both media, and the state of polarization of the incident radiation.

The expressions for ϕ_p^r, ϕ_p^t, ϕ_s^r, and ϕ_s^t for any interface can be determined in a straightforward manner from equations (55) through (58). However the algebra involved is cumbersome and it was more informative to investigate the behavior of these functions for typical values of the optical constants of an absorbing layer on an absorbing substrate. The calculation of these functions was relatively straightforward since a computer which could perform algebraic operations with complex numbers was available. *

---

*The calculations were performed on the Control Data Corporation 1604-A digital computer at ORNL.

In all the calculations the medium from which the radiation was incident was vacuum. The index of refraction and extinction coefficient of the layer were designated n_1 and k_1, respectively, while the region behind the layer was characterized by n_2 and k_2.

The first case considered is a self-supporting layer (i. e., $n_2 = 1.0$, $k_2 = 0$) with $n_1 = 1.5$ and $k_1 = 0$, .1, .5, and 1.0. The phase shift of component I, reflected from the front surface of the layer, is shown as a function of θ in Fig. 13. The phase jump is expressed in degrees instead of radians and the subscripts "s" and "p" have been replaced by appropriate symbols. For a transparent layer ($k_1 = 0$) and radiation polarized with its electric vector in a plane perpendicular to the plane of incidence, ϕ is $-180°$ for all angles of incidence, while for radiation polarized with its electric vector parallel to the plane of incidence, it is $-180°$ below Brewster's angle and $0°$ above Brewster's angle. For absorbing films ($k_1 > 0$) ϕ takes on values between $0°$ and $-180°$, and is a function of k_1 and θ as well as the polarization. The phase shifts on reflection from the rear surface of the layer expressed as a function of the exterior angle of incidence θ (not the interior angle, θ') is shown in Fig. 14. The shape of this set of curves is exactly the same as those shown in Fig. 13, but all values are displaced by $180°$. Note that Brewster's angle on the rear surface occurs at the same angle as Brewster's angle on the front surface when θ (rather than θ') is used in both cases. This is an elementary consequence of Snell's law.
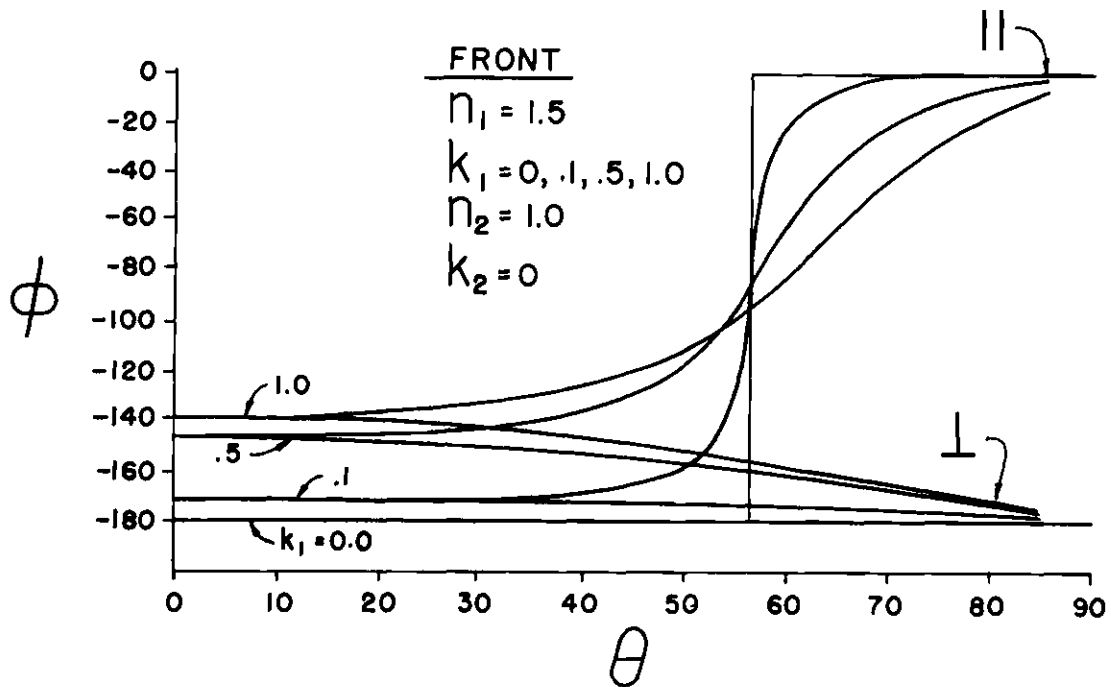
Figure 13. Phase Shifts on Reflection from the Front Surface of a Layer
as a Function of Angle-of-Incidence, Extinction Coefficient,
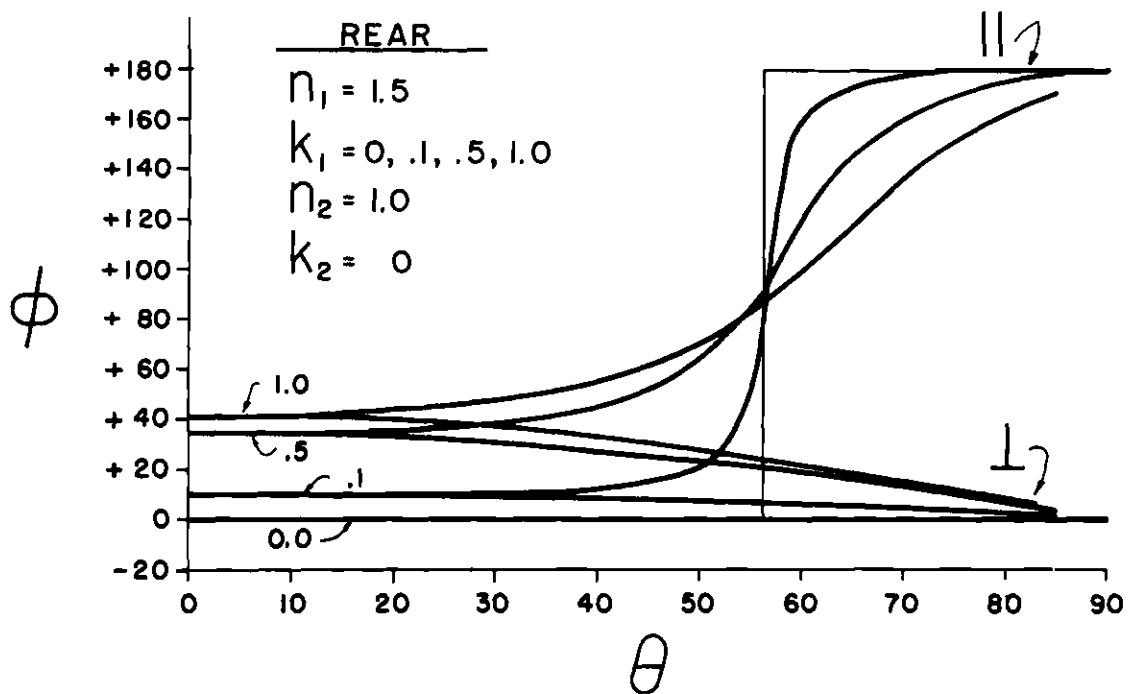and Polarization of the Incident Radiation

Figure 14. Phase Shifts on Reflection from the Rear Surface of a Self-
Supporting Layer as a Function of Angle-of-Incidence, Extinction
Coefficient, and Polarization of the Incident Radiation

Figure 15 shows the net phase shift for reflection from a free-standing

layer. As mentioned earlier the difference in phase between I and II due to

reflection at the front and rear of the layer, respectively, is exactly 180°.

The difference between 180° and the values shown in Fig. 15 is due to phase

shifts on transmission (i. e., when II enters and leaves the layer). The

important observation to be made about Fig. 15 is that for $k_1 < .1$, the net

phase change is very near 180° regardless of the angle of incidence or the

polarization. However, if interference patterns are to be observed, the

layer must be on the order of a wavelength thick, and thus, if there is to

be sufficient intensity to produce interference, k must be less than .1.

Thus for a self-supporting layer and the range of k for which interference is

possible, P is very nearly equal to -.5, its value for a transparent material.

This observation, while useful for materials like aluminum which can be

made into free-standing films, is not applicable to sodium, since sodium

films must be supported on substrates.

The next case to be considered is an absorbing film ($n_1 = 1.5$, $k_1 = 0$,

.05, .1) on a transparent substrate ($n_2 = 2.0$, $k_2 = 0$). The extinction

coefficient of the layer has been restricted to values small enough to permit

interference. The net phase shifts for this system are shown in Fig. 16.

The significant feature of this figure is the difference in the phase shift

for parallel and perpendicularly polarized radiation for angles greater than

Brewster's angle on the front surface. For the optical constants used to
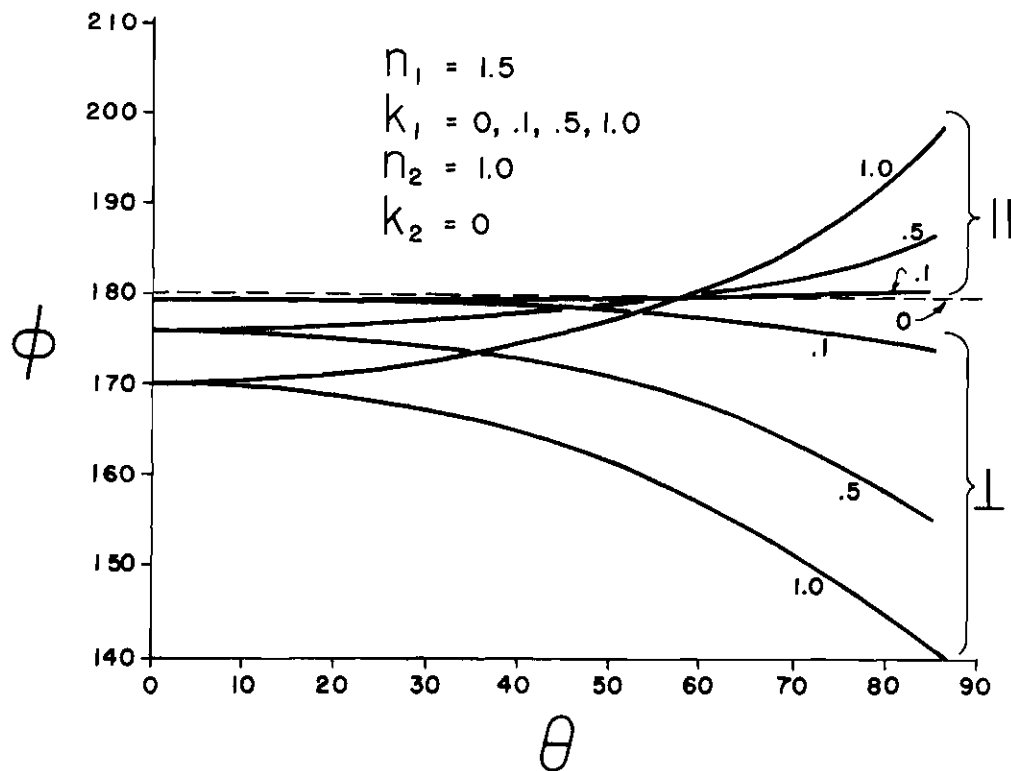
Figure 15. Net Phase Shift on Reflection from a Self-Supporting Layer as a Function of Angle-of-Incidence, Extinction Coefficient, and Polarization of the Incident Radiation
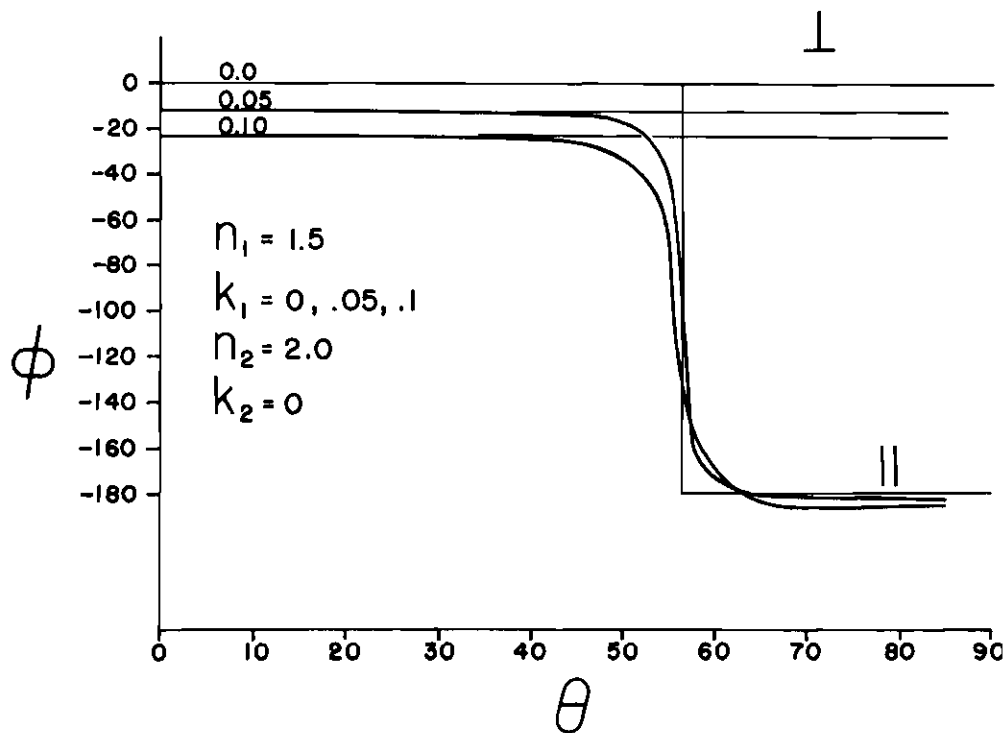
Figure 16. Net Phase Shifts on Reflection from a Layer Supported on a Transparent Substrate as a Function of Angle-of-Incidence, Extinction Coefficient of the Layer, and Polarization of the Incident Radiation

generate Fig. 16, there is no exterior angle θ which causes component II

to be reflected from the rear surface at the Brewster's angle of that

surface. For other sets of optical constants there could be Brewster's

angles at both surfaces in which case there would be changes of approximately

180° in the net phase shift of parallel polarized radiation for both of these

angles. Thus the use of parallel polarized radiation causes considerable

complication in the interpretation of interference patterns. However, if

the incident radiation is unpolarized or if the perpendicular component is more

intense than the parallel component, the interference pattern may be

analyzed by assuming that the radiation is polarized perpendicular to the plane

of incidence. This assumption is based on the fact that the reflectance of

parallel polarized radiation from a surface is much less than the reflectance

of perpendicularly polarized radiation for angles of incidence near the

Brewster's angle of the surface. Thus for the system shown in Fig. 16

little parallel-polarized radiation would be reflected from the front

surface for θ near 56°, the Brewster's angle of that surface, while as θ

approaches 90°, θ' will move nearer the Brewster's angle of the rear

surface, and reflectance of parallel-polarized radiation from that surface

would decrease. Near normal incidence, the reflectance of parallel-polarized

radiation is nearly as great as the reflectance of perpendicularly-polarized

radiation. However, the net phase change is nearly the same for both

components in this region.

Figures 17 and 18 show the net phase change $\underline{vs}$ θ for 584 Å and 736 Å radiation reflected from a sodium film deposited on a glass substrate. The optical constants of aluminum and glass used in the calculation were determined by Madden $\underline{et}$ $\underline{al}$. (43) by the two-angle method. The reflectance of unoxidized aluminum was found by measuring reflectance as a function of time after evaporation and extrapolating to zero time. Interference patterns similar to the ones shown in Figs. 9 and 10 have been observed for aluminum films at 584 Å and 736 Å. The index of refraction of aluminum which was determined from these patterns by assuming that the net phase shift was zero was .72 at 584 Å at .47 and 736 Å (42, 44). However, Figs. 17 and 18 show that the net phase change is about -150° for 736 Å and between -120° and -140° for 584 Å. When the values of the phase shifts shown in Figs. 17 and 18 are used with the same interference data the index of refraction is found to be .708 at 584 Å and .454 at 736 Å in good agreement with the values of .71 and .455 determined by Madden $\underline{et}$ $\underline{al}$. (43) at these wavelengths.

It was pointed out above that if the radiation incident on a film is unpolarized or predominantly perpendicularly polarized, only the perpendicularly polarized component need be considered in analyzing interference patterns. In the work on aluminum (43, 44) the incident radiation was assumed unpolarized since normal incidence monochromators were used. However, in the present work the incident radiation is polarized since a Seya-Namioka
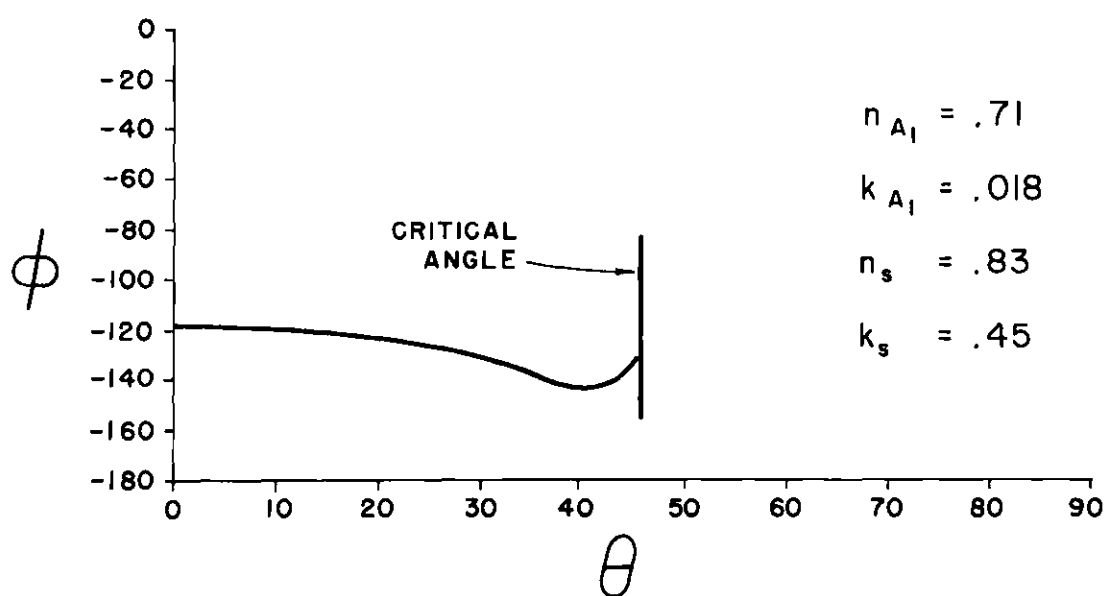
Figure 17. Net Phase Shift of 584 Å Radiation Reflected from an Aluminum Film Deposited on a Glass Substrate as a Function of Angle of Incidence
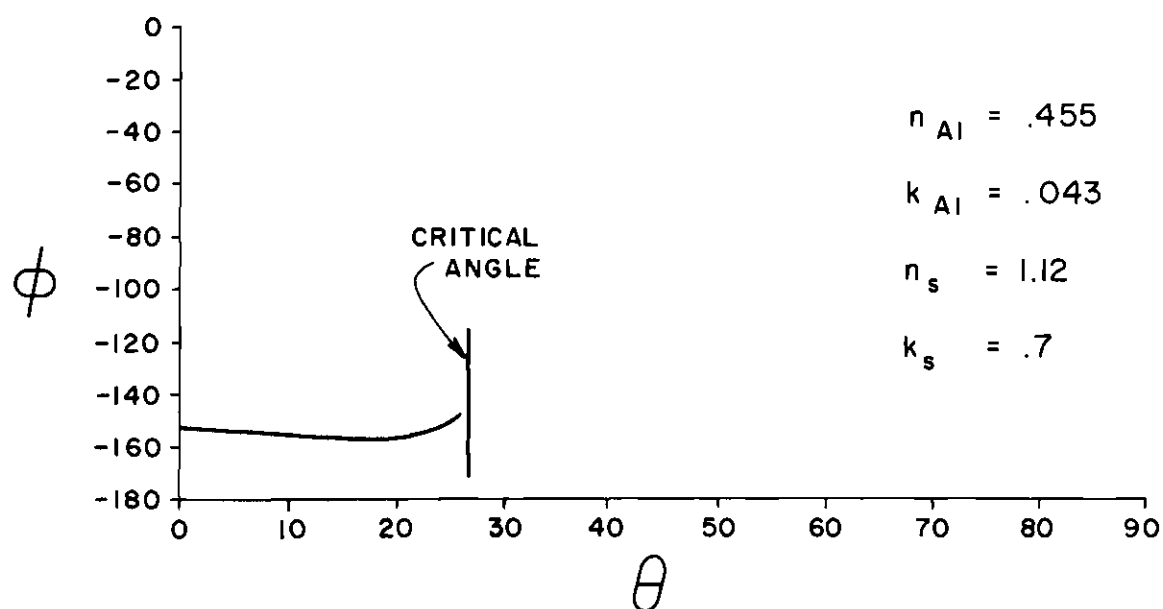
Figure 18. Net Phase Shift of 736 Å Radiation Reflected from an
Aluminum Film Deposited on a Glass Substrate as a Function
of Angle of Incidence

monochromator was used. Figure 19 shows the ratio of the intensity of
parallel-polarized radiation to perpendicularly-polarized radiation as a
function of wavelength reported by Hamm et al. (45) for the monochromator
and grating used in this work. For all wavelengths less than 2000 Å, the
ratio is less than 1. Thus, in this work both the monochromator and the
sodium film acted as filters which discriminated in favor of perpendicularly-
polarized radiation.

The value of P for each order of interference was computed from
measured values of the optical constants of quartz and approximate values
of the optical constants of sodium. The optical constants of the quartz
substrate were determined by the two-angle method. An approximate value
of the index of refraction of sodium was obtained from the intersection of
the ordinate with the line which determined the orders of interference (e.g.,
Line II of Fig. 12). The method of least squares was used to fit a straight
line of the form of equation (69) to the points whose ordinates are $\sin^2 \theta$
and whose abscissas are the corresponding values of $(N - P)^2$. The inter-
section of this line with the ordinate gave a new value of the index of
refraction of sodium. This value of n was used to calculate P, and the
process was repeated until the value of n used to compute P agreed with the
value of n computed from these P's. The iteration converged rapidly. The
calculations were performed on the Oak Ridge CDC 1604-A digital computer.

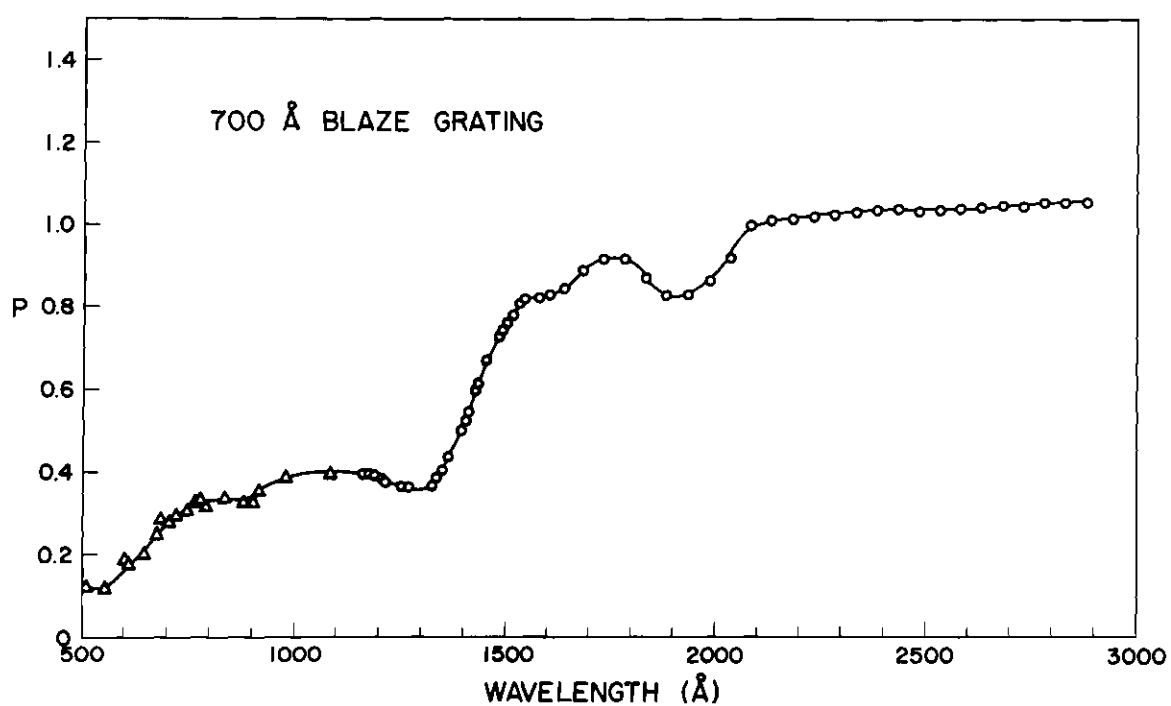The final value of n was insensitive to the value of k of sodium and

Figure 19. Polarization of Grating Versus Wavelength

the values of n and k of quartz used in the calculation of P. Figure 20 shows

P(θ) for 836 Å. The calculations were made for n(Na) = .935, n(qz) = 1.24,

k(qz) = .68 and two values of k(Na) , .005 and .01. Figure 20 shows that

there is very little difference in the value of P calculated for the two values

of k(Na). Tables 3, 4, 5, and 6 show the effect on the calculated value of

the index of refraction of sodium at 836 Å caused by varying one of the four

parameters, n(Na), k(Na), n(qz), and k(qz), used in the calculation of P.

However, as noted above, in determining n(Na) an iteration was performed

until the two values of n(Na) agree. The values of the indices of refraction

of two sodium films obtained by the interference method are shown in Table

1. The values of n(Na) for the two films agree with each other and with the

values obtained by the critical-angle method. The appendix contains a

representative sample of the reflectance measurements on which the

results given in Table 1 are based.

The formulation of oxide on the surface of the sodium does not

appear to affect the value of the index of refraction determined by the

interference method. Figure 21 shows the reflectance of 1216 Å radiation

from a sodium film 20 minutes, 3 hours, and 24 hours after the film was

formed. The formation of oxide on the vacuum-sodium interface reduced

the reflectance of the film between the 20 minute and 3 hour measurements.

However, little change in reflectance is observed between the 3 hour and

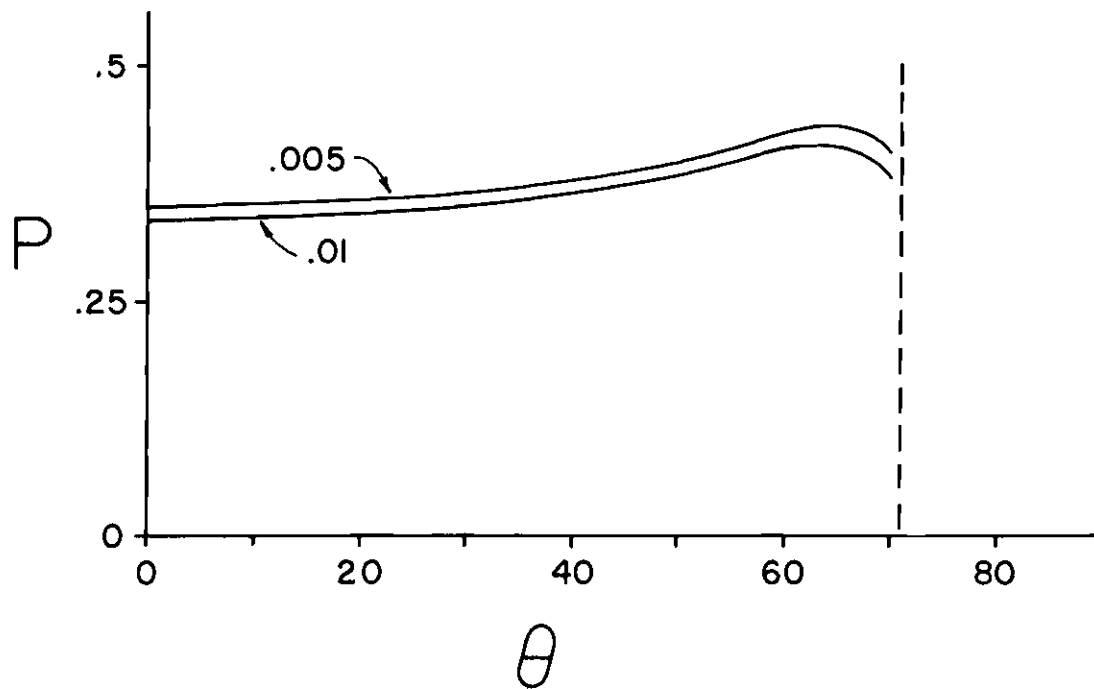24 hour measurements. This indicates that the oxide layer reached a terminal

Figure 20. Phase Shifts of 836 Å Radiation Reflected from a Sodium
Film Deposited on a Quartz Substrate as a Function of Angle
of Incidence

Table 3

Sensitivity of the Calculated Value of the Index of Re-
fraction of Sodium to Variations in the Value of the Index
of Refraction of Sodium Used in the Computation of the
Phase Shifts (λ = 836 Å)

$k(Na) = 0.005$, $n(Qz) = 1.24$, $k(Qz) = 0.68$

$n(Na)$ (Input)	$n(Na)$ (Output)
.87	.9586
.90	.9449
.935	.9345
.97	.9358
1.00	.9408

Table 4

Sensitivity of the Calculated Value of the Index of Refrac-
tion of Sodium to Variations in the Value of the Extinction
Coefficient of Sodium Used in the Computation of Phase
Shifts (λ = 836 Å)

$n(Na) = .935$, $n(Qz) = 1.24$, $k(Qz) = 0.68$

$k(Na)$	$n(Na)$
.001	.9341
.005	.9345
.01	.9350
.015	.9354
.02	.9358

Table 5. Sensitivity of the Calculated Value of the Index of Refraction of
Sodium to Variations in the Value of the Index of Refraction of
the Substrate Used in the Computation of Phase Shifts ($\lambda = 836$ Å)

$n(Na) = .935, \quad k(Na) = 0.01, \quad k(Qz) = 0.68$

$n(Qz)$	$n(Na)$
1.1	.9350
1.24	.9350
1.5	.9349

Table 6. Sensitivity of the Calculated Value of the Index of Refraction of
Sodium to Variations in the Value of the Extinction Coefficient
of the Substrate Used in the Computation of Phase Shifts ($\lambda = 836$ Å)

$n(Na) = .935, \quad k(Na) = 0.01, \quad n(Qz) = 1.24$

$k(Qz)$	$n(Na)$
.50	.9350
.68	.9350
.90	.9349
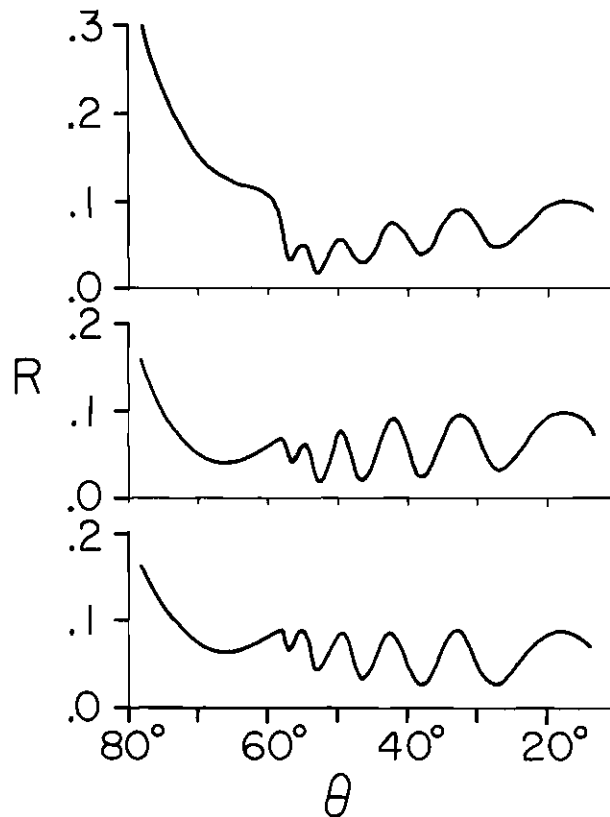
Figure 21. Reflectance of a Sodium Film _Versus_ Angle-of-Incidence for 1216 Å Radiation 20 minutes, 3 hours, and 24 hours after Evaporation

thickness. Figure 21 also shows that the positions of the interference fringes are not affected by the growth of the oxide layer. Thus the terminal thickness of the oxide must be small in comparison with the thickness of the sodium film, which exceeded 4000 Å. That is, the oxide layer does not seriously affect the term in equation (68) which depends on T, the thickness of the film. The effect of the oxide layer on the phase changes for reflections from or transmission through the vacuum-sodium interface cannot be computed since the optical constants of the oxide are not known. However, a sodium film deposited on a quartz hemi-cylinder produced interference patterns when radiation of wavelength greater than 1700 Å was incident on the film from the quartz side as well as from the vacuum side. If the oxide on the vacuum-sodium surface affected the calculated values of n, a different value of n would be expected from the interference pattern of radiation incident from the quartz side of the film since the effect of the oxide would be different for this case. However, the index of refraction determined from radiation incident from the quartz side of the film agreed within experimental accuracy with the value determined from measurements made when the radiation was incident from the vacuum side of the film. Thus the values of the index of refraction given by the interference method appear to be unaffected by the oxide layer.

The Extinction Coefficient

The extinction coefficient of sodium was found by comparing the

reflectance of unoxidized sodium surfaces with theoretical reflectances

computed for different values of n and k. The reflectance of 1849 Å

radiation from a sodium film deposited on the quartz hemi-cylinder was

shown in Fig. 6. The measured reflectance was normalized by comparison

with the reflectance of the quartz-vacuum interface and background

corrections were made as described in chapter IV. The normalized reflec-

tances determined from Fig. 6 for 10 values of θ are shown as points in

Fig. 22. The diamond shown in Fig. 22 is the reflectance which was used to

determine the background. The lines shown in Fig. 22 are the reflectances

for polarized radiation (see Fig. 19) reflected from a surface with a

relative index of refraction of .35 and relative extinction coefficients of

0, .01, .02, and .03. The experimental values of reflectance are compared

with reflectances computed for n equal to .35 since the critical angle at

this wavelength is 20.5°. The figure shows that the experimental points

come close to fitting the theoretical curve for which k = .02.

The extinction coefficient of sodium is found by multiplying the

relative value obtained from measurements made on the quartz-sodium inter-

face by the index of refraction of quartz (10). The uncertainty in the

relative value is taken to be ± .003, because of the uncertainty in the

measured reflectances indicated by the error bars in Fig. 22. Thus for

1849 Å radiation, the extinction coefficient of sodium is .031 ± .005. Values

of k for 1849 Å and other wavelengths and the corresponding values of ϵ_2
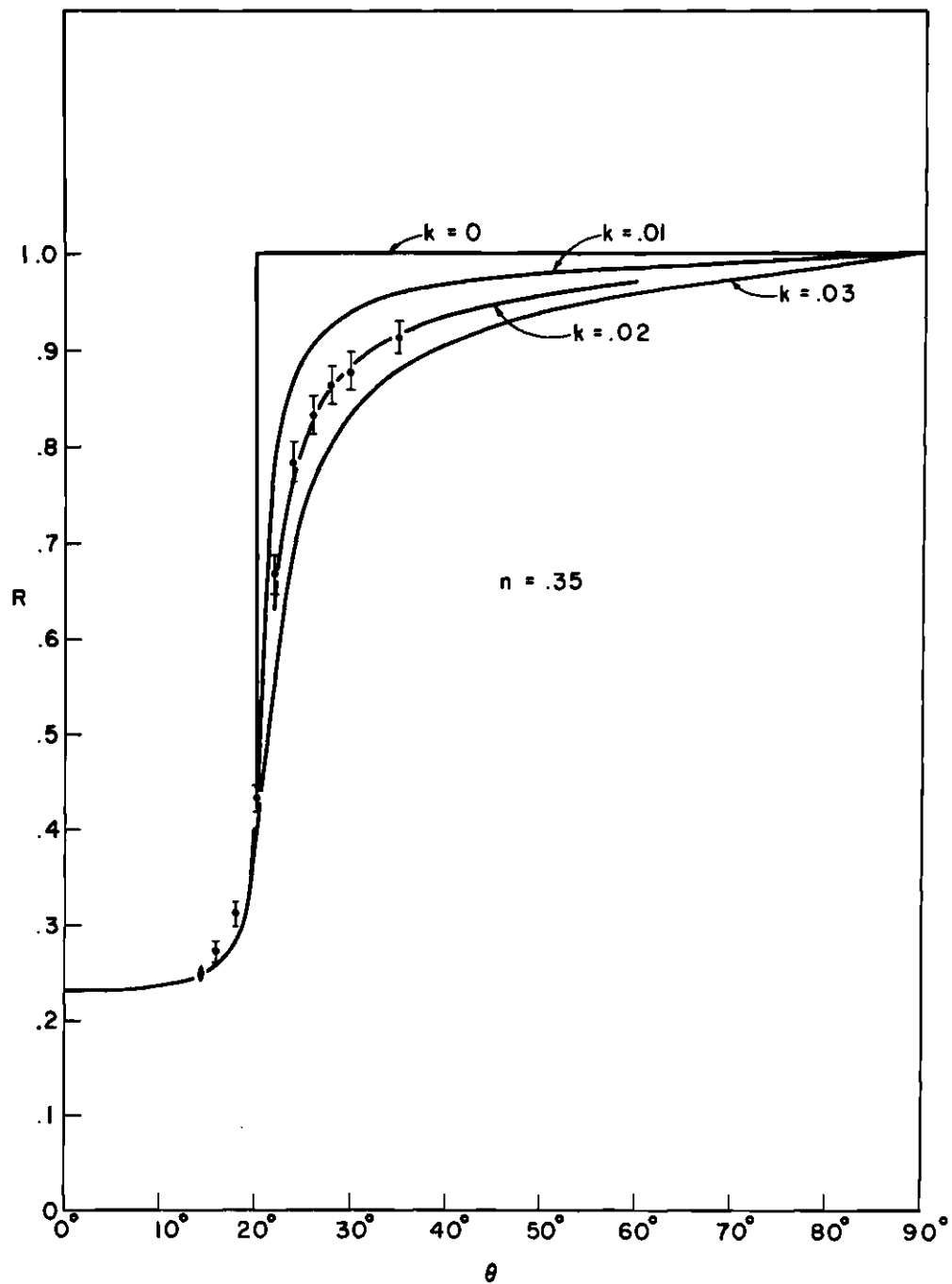
are given in Table 7.

Figure 22. Theoretical Reflectance from a Semi-Infinite Layer of Index-of-Refraction .35 and Experimentally Determined Reflectance of 1849 Å Radiation from a Quartz-Sodium Interface. The reflectance used to calculate background is indicated as a diamond

Table 7. Extinction Coefficient, k, and Imaginary Part of the
Dielectric Constant, ϵ_2, of Sodium

λ (Å)	k	ϵ_2
2000	.036 ± .003	.029 ± .003
1950	.034 ± .005	.031 ± .005
1849	.031 ± .005	.033 ± .005
1743	.023 ± .008	.028 ± .01

CHAPTER VI

DISCUSSION OF RESULTS

According to equation (14) $\epsilon_1 = n^2 - k^2$. However, Table 7 shows that k is less than .04 at 2000 Å and according to equations (22, 23, and 49), k decreases at shorter wavelengths. Table 1 shows that n is .404 at 2000 Å and increases at shorter wavelengths. Thus the value of k^2 is never greater than 1% of the value of n^2 for λ less than 2000 Å. Thus it is a good approximation to take ϵ_1 equal to n^2 in this wavelength region. The last column in Table 1 gives the value of ϵ_1 obtained by squaring the value of n given in the adjacent column.

The values of ϵ_1 obtained in the present work may be conveniently compared with theory and with the near-ultraviolet, visible, and infrared data of Ives and Briggs (10) and Mayer and Hietel (17, 20) by plotting $\ln(1 + 4\pi\varkappa\alpha_T - \epsilon_1)$ and $\ln(1 + 4\pi\varkappa\alpha_1 - \epsilon_1)$ versus $\ln\hbar\omega$, as shown in Fig. 23. The triangles in Fig. 23 were obtained from Mayer and Hietel's values for ϵ_1, the crosses from Ives and Briggs' values, and the circles from Table 1. The datum for 420 Å cannot be plotted in Fig. 23 since ϵ_1 is greater than $1 + 4\pi\varkappa\alpha_1$ at this wavelength. All of the points except the three circles near 30 eV lie close to a straight line of slope -2 in agreement with Eqs. (33) and (37) which can be rewritten as
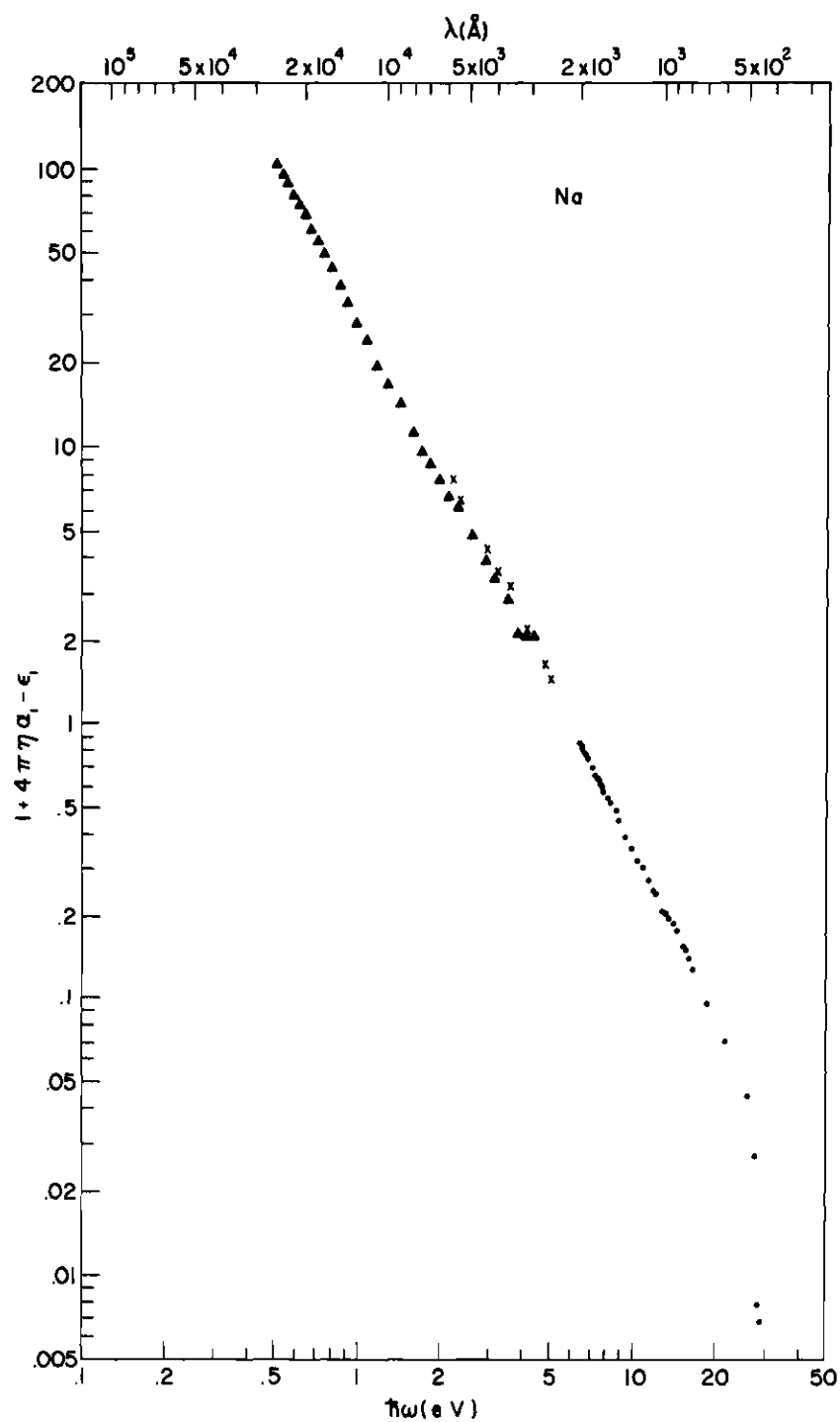
Figure 23. Logarithm of $1 + 4\pi\kappa\alpha_1 - \epsilon_1$ Versus Logarithm of Photon Energy. Mayer and Hietel, ▲; Ives and Briggs, X; present work, ●.

$$\ln(1 + 4\pi\alpha_T - \epsilon_1) = 2\ln(\hbar\omega_a) - 2\ln(\hbar\omega) \tag{71}$$

and

$$\ln(1 + 4\pi\alpha_1 - \epsilon_1) = 2\ln(\hbar\omega_b) - 2\ln(\hbar\omega) \quad . \tag{72}$$

As mentioned in Chapter II, equation (71) is applicable from .02 eV to 1.2 eV and equation (72) is applicable from 2.2 eV to just below 30 eV. In the anomalous region from 1.2 to 2.2 eV, there is a slight break in the line.

A similar comparison of the experimental values of ϵ_2 can be made by plotting $\ln\epsilon_2$ versus $\ln\hbar\omega$ as shown in Fig. 24. Again, triangles represent the data of Mayer and Hietel, crosses show the values determined by Ives and Briggs, and circles are the values given in Table 7. Mayer and Hietel's values of ϵ_2 for $\hbar\omega < 1.2$ eV fit a straight line with a slope of minus three. This is just the behavior predicted by equation (23) if γ (and thus the relaxation time, $\tau = 1/2\pi\gamma$) is independent of photon energy. The value of τ determined from the data of Mayer and Hietel is 5.0×10^{-14} sec., in reasonable agreement with the value of 3.3×10^{-14} sec. estimated from the static conductivity of sodium (34).

Between 1.2 eV and 2.2 eV there is a peak in ϵ_2 which cannot be explained by the one-electron theory since the threshold for direct interband transitions is 2.2 eV.

Several workers (22, 23, 24, 25, 26, 27, 28) have suggested possible causes for this anomalous peak, but at the present time the question is unresolved.
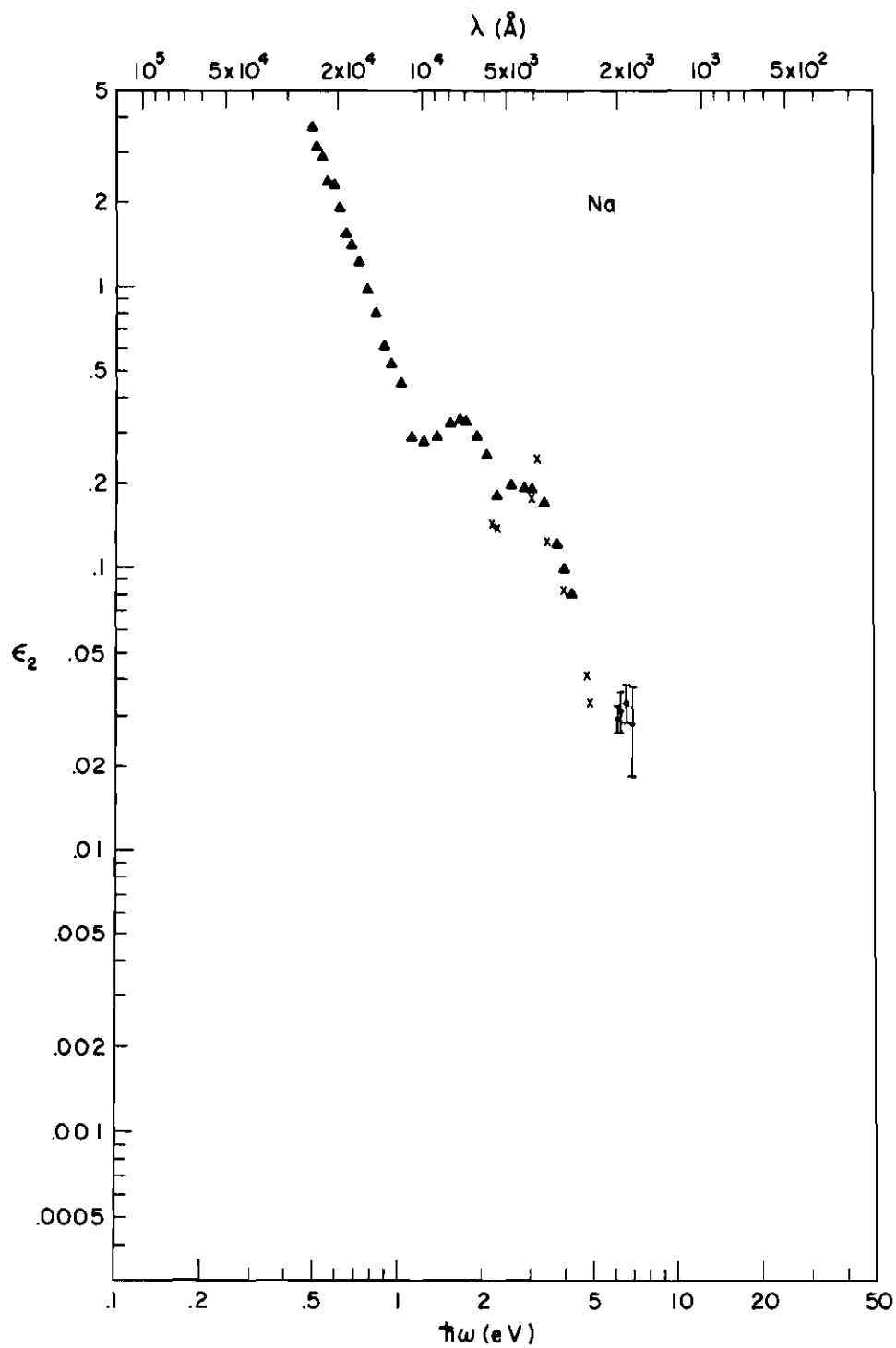
Figure 24. Logarithm of ϵ_2 Versus Logarithm of Photon Energy. Mayer and Hietel, ▲; Ives and Briggs, X; present work, ●.

For photon energies greater than the threshold for direct-interband transitions at 2.2 eV there is a second peak in ϵ_2. This peak is present in the data of both Mayer and Hietel and Ives and Briggs. After the initial rise associated with the direct interband transitions, ϵ_2 decreases again with a slope of approximately minus three.

There appears to be a third peak in ϵ_2 between 6 eV and 7 eV. This peak may be due to transitions from the conduction band to the second unoccupied band. Band calculations (14, 16) indicate that the threshold transitions are from states on a Λ symmetry axis. The threshold energy is about 5.3 eV.

The values of ω_a, ω_b, and ω_p may be found from Fig. 23, but better accuracy is obtained by a somewhat different procedure. Equations (33) and (37) can be expressed in terms of λ instead of ω, giving

$$\epsilon_1 = 1 + 4\pi\kappa\alpha_T - \lambda^2/\lambda_a^2 \quad , \tag{73}$$

where

$$\lambda_a^2 = \frac{\pi c^2}{\kappa_c e^2} \, m_a \quad , \tag{74}$$

and

$$\epsilon_1 = 1 + 4\pi\kappa\alpha_1 - \lambda^2/\lambda_b^2 \quad , \tag{75}$$

where

$$\lambda_b^2 = \frac{\pi c^2}{\kappa_c e^2} \, m_{opt} \quad . \tag{76}$$

Since sodium is mono-valent, κ is equal to κ_c.

The values of ϵ_1 determined in the present experiment and the two

values determined by Wood (5) are plotted versus λ^2 in Fig. 25. All of the

points determined in the present work lie close to a straight line except for

the four points which are near the threshold for the excitation of core

electrons. This threshold is indicated by an arrow in Fig. 25. The solid line

shown in the figure was fitted to the experimental points by the method of

least squares. The four points near the excitation threshold were not used

in the determination of this line.

The parameters of equation (75) can be determined from the line in

Fig. 25. The value of $1 + 4\pi\varkappa\alpha_1$ is given by the extrapolation of the line

through the experimental points to $\lambda = 0$. This extrapolation gives $1.03 \pm$

0.02 for $1 + 4\pi\varkappa\alpha_1$ or 0.03 ± 0.02 for $4\pi\varkappa\alpha_1$. The value of λ_b is given by the

slope of the line through the data points, and m_{opt} is computed from equation

(76). The result, expressed as the ratio of m_{opt} to m, the rest mass of a

free electron, is 1.06 ± 0.05. The plasma wavelength, λ_p, is determined by

the extrapolation of the line through the data points to $\epsilon_1 = 0$. The

extrapolation shown in Fig. 25 gives $\lambda_1 = 2185 \pm 25$ Å.

Table 8 summarizes the dielectric parameters of sodium obtained in

this and other experiments. The quantities λ_a, λ_b, and λ_p have been con-

verted to equivalent photon energies. The optical measurements of

Hodgson (13), Mayer and H\.ietel (17, 20), and Ives and Briggs (10) were made

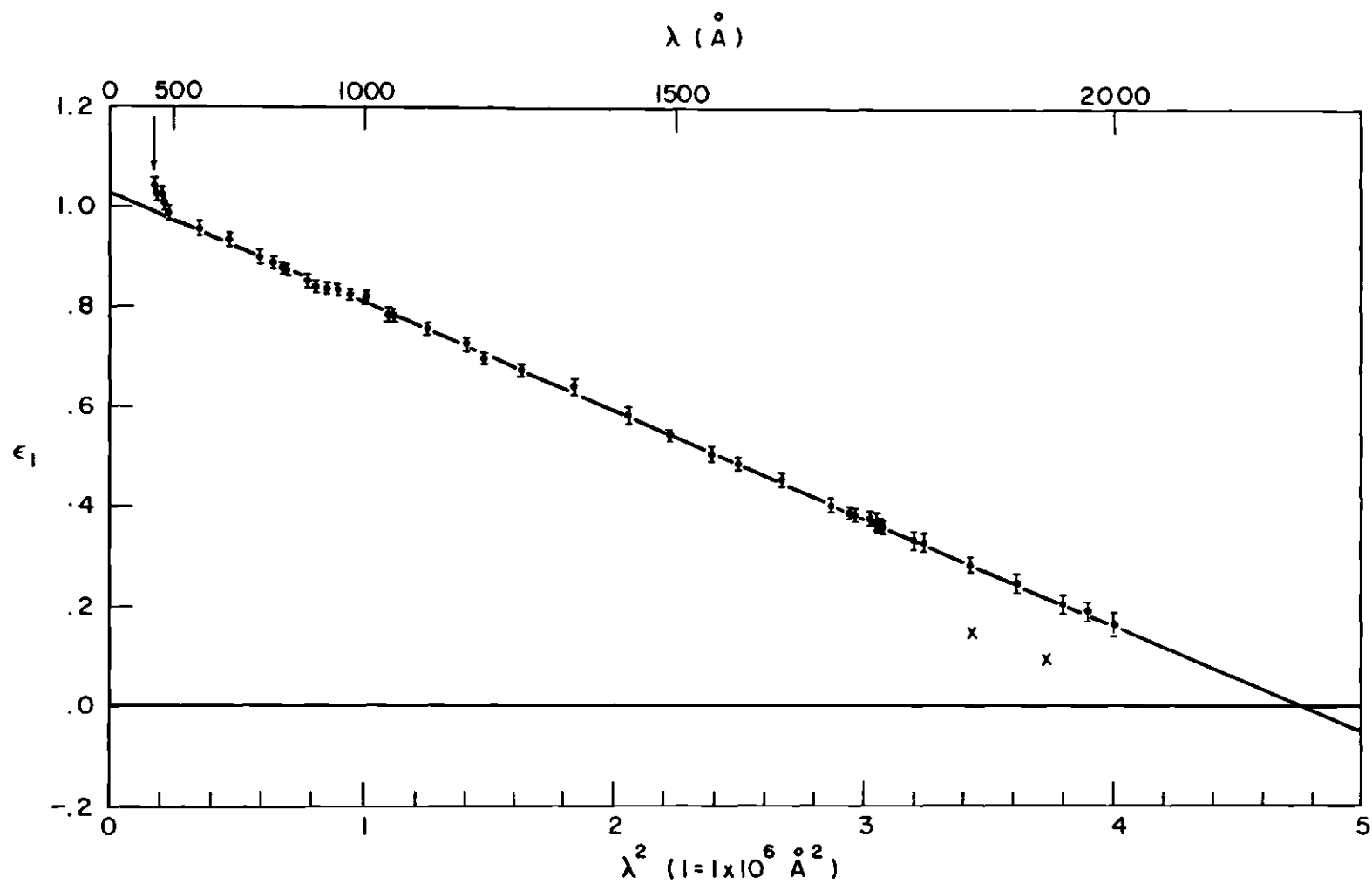for photon energies less than the plasma energy, $\hbar\omega_p$. The values they

Figure 25. Real Part of the Dielectric Constant of Sodium <u>Versus</u> λ^2
for Wavelengths Between 420 and 2000 Å. Wood, X; present
work, •.

Table 8. Polarizabilities, Effective Electron Masses and the Plasma Energy of Sodium

	$4\pi\varkappa\alpha_1$	$4\pi\varkappa\alpha_0$	m_a/m	$\hbar\omega_a$ (eV)	m_{opt}/m	$\hbar\omega_b$ (eV)	$\hbar\omega_p$ (eV)
Cohen's Analysis of Ives and Briggs Data (12, 10) (Ellipsometry)	.1 ± .08				1.01 ± .02	5.90	5.62
Hodgson (13) (Ellipsometry)			1.08 ± .01	5.7			
Mayer and Hietel (17, 20) (Ellipsometry)	.15 ± .1		1.27 ± .02	5.27	1.17 ± .03	5.49	5.49*
Present Work (Critical-Angle and Interference)	.03 ± .02				1.06 ± .05	5.77	5.68 ± .06
Tessmann (51) (Polarizability of Sodium Ions in Sodium Halide Crystals)		.13					
Robins and Best[†](46) (Electron-Energy Loss)							5.69 ± .08
Swan[†](47) (Electron-Energy Loss)							5.67 ± .05
Kunz(48) (Electron-Energy Loss)							5.71 ± .1
Sueoka(49) (Electron-Energy Loss)							5.60 ± .05

*Mayer and Hietel determined $\hbar\omega_p$ from the peak of the energy loss function, $(2nk)/(n^2 + k^2)^2$. They determined n and k in the region near $\hbar\omega_p$ by extrapolations using their data, 2 points determined by Ives and Briggs (10), and two points determined from the reflectance measurements of Wood (5). The plasma energy may be computed directly from the data of Mayer and Hietel by requiring ϵ_1 ($\hbar\omega$) = 0. Then $(\hbar\omega_p)^2 = (\hbar\omega_b)^2/(1 + 4\pi\varkappa\alpha_1)$. Substituting the values of $\hbar\omega_b$ and $4\pi\varkappa\alpha_1$ given above gives $\hbar\omega_p = 5.1 \pm .3$ eV.

†The values of $\hbar\omega_p$ reported by Robins and Best, and Swan have been reduced 3 per cent to account for dispersion effects. This correction has been discussed by Powell (5 0).

obtained from $\epsilon_1(\lambda)$ by analyses similar to the one described above are given

in Table 8. The data of Mayer and Hietel include photon energies both less

than and greater than the threshold for interband transitions. Thus their

results give values of the parameters of both equations (73) and (75). Mayer

and Hietel found $\hbar\omega_p$ from the peak of the energy loss function, $(2nk)/(n^2+k^2)^2$.

The values of n and k used to calculate the energy loss function near the

plasma wavelength were obtained by extrapolations fitted to their data, two

points determined by Ives and Briggs, and two points determined from the

reflectance measurements made by Wood.

The values of α_1 and m_{opt} reported by Mayer and Hietel are

significantly larger than the values found in the present experiment. Mayer

and Hietel found α_1 equal to 0.15 ± 0.1 and m_{opt}/m equal to 1.17 ± 0.03, while

we found 0.03 ± 0.02 and 1.06 ± 0.05, respectively. However, these differ-

ences may be due to the approximation used to derive equation (37). As ω in-

creases, the summation in the third term of equation (35) includes fewer states

so the contribution of this term decreases. However, the summation in the

fifth term of equation (35) includes more states and thus the contribution of

this term increases in magnitude. Thus, as ω increases, α_1 decreases and

ω_b increases, causing m_{opt} to decrease in qualitative agreement with the

experimental results.

Confusion exists in the comparison of the plasma energy obtained

from electron-energy-loss experiments with the plasma energies obtained

from optical data. The difficulty is that $\hbar\omega_a$, $\hbar\omega_b$, and $\hbar\omega_p$ are all often

referred to as the plasma energy. However, $\hbar\omega_a$ and $\hbar\omega_b$ cannot be compared

with the electron-energy-loss results since they do not include the effect of

core and valence-electron polarizability. The polarizabilities increase ϵ_1

and thus decrease the plasma energy in a real metal. The plasma energy is

determined by the condition $\epsilon^*(\omega) = 0$ (33). If damping effects are small,

the condition for a plasma oscillation becomes $\epsilon_1 = 0$ (33). Thus, $\hbar\omega_p$ is

the energy to be compared with the electron-energy-loss data. The values of

$\hbar\omega_p$ obtained in the present work agree with the electron-energy-loss

experiments of Robins and Best (46), Swan (47), Kunz (48), and Sueoka (49)

within the limits of experimental accuracy. The values of $\hbar\omega_p$ given by

Robins and Best and Swan have been decreased 3 per cent to allow for

dispersion of the energy loss with scattering angle. This correction has been

discussed by Powell (50).

The most serious disagreement found in Table 8 is in the value of the

polarizability of the ion core. According to Cohen (12), α_1 should be

greater than α_o. However, the value of α_1 obtained in the present work is

significantly less than the value of α_o given by Tessman et al. (51, 12) who

measured the polarizability of sodium ions in sodium halide crystals. Our

results are in somewhat better agreement with the earlier work of Born and

Heisenberg (52), Fajans and Joos (53), and Pauling (54) who found $4\pi\kappa\alpha_o$ to be

0. 07, 0. 06, and 0. 06, respectively.

CHAPTER VII

CONCLUSIONS

Accurate values of the index of refraction of a metal for photon

energies greater than the metal's plasma-energy can be obtained by both

the interference and the critical-angle methods even if the surface of the

metal is covered by a thin layer of oxide. Proper analysis of interference

data must take into account phase shifts on reflection from or transmission

through the surfaces of the metal film. Calculations show that for a self-

supporting film with extinction coefficient less than .01, the phase shifts

are, to a good approximation, the same as the phase shifts for a dielectric

layer. However, for supported films, polarization effects and the index of

refraction and extinction coefficient of the substrate must be considered.

The reflectance of unoxidized metallic surfaces can be measured by

use of a hemi-cylinder in the wavelength region in which the hemi-cylinder is

transparent. The extinction coefficient of the metal can be determined

from the reflectance measurements made on the unoxidized surface.

The measured values of the index of refraction and extinction

coefficient can be used to compute the real and imaginary parts of the

dielectric constant. The real part of the dielectric constant of sodium

agrees with the expressions derived by Cohen (12) from the independent-

particle quantum-mechanical model of metallic structure. From the values

of ϵ_1 measured for photon energies greater than the plasma energy of sodium,

the optical-effective mass was found to be $1.06 \pm .05$ times the rest mass

of a free electron and $4\pi\varkappa\alpha_1$ was found to be $.03 \pm .02$. The larger values of

m_{opt} and $4\pi\varkappa\,\alpha_1$ reported by Mayer and Hietel (17, 20) for photon energies

less than the plasma energy were shown qualitatively to be a consequence of

the approximations used by Cohen (12). The value of $4\pi\varkappa\alpha_1$ found in the present

work showed that the value of .13 which had been reported for $4\pi\varkappa\alpha_o$ by

Tessman (51) was too large. Better agreement was noted between the present

results and the values of .07, .06, and .06 reported by Born and Heisenberg

(52), Fajans and Joos (53), and Pauling (54), respectively.

The wavelength at which $\epsilon_1 = 0$, found by extrapolation of the values

of ϵ_1 measured in the present work, is 2185 Å $\pm$ 25 Å. Thus, the plasma

energy of sodium is $5.68 \pm .06$ eV. This value of the plasma energy agrees

within the limits of experimental accuracy with the values of 5.69 eV $\pm$

.08 eV, 5.67 eV $\pm$ .05 eV, 5.71 eV $\pm$ .1 eV and 5.60 eV $\pm$ .05 eV reported by

Robins and Best (46), Swan (47), Kunz (48) and Sueoka (49) respectively.

CHAPTER VIII

RECOMMENDATIONS

The optical constants of potassium, rubidium, and cesium have been

measured by Ives and Briggs (10) and Mayer and his co-workers (17, 18, 19, 21)

in a portion of the region below their plasma wavelengths (which are approxi-

mately 3000 Å, 4000 Å, and 4300 Å, respectively). These measurements

indicate that the critical angle method can be used to determine the index of

refraction of potassium, rubidium and cesium in this wavelength region even

though the effects of interband transitions are more pronounced in these

metals than in sodium. Interference measurements may also be possible

particularly in the case of potassium since Wood (4) has observed interference

in the reflectance from potassium films as a function of wavelength and film

thickness. It should also be possible to determine the extinction coefficients

of K, Rb, and Cs between 1700 Å and the plasma wavelength of each metal

from reflectance measurements made with a quartz hemi-cylinder. Deter-

mination of the optical constants of K, Rb, and Cs in the wavelength region

from 2537 Å (Ives and Briggs (10) shortest wavelength) to the plasma wave-

length of each metal would permit comparison of the method used in the

present work with the polarimetric methods used by Mayer and Ives and

Briggs. In addition, measurement of the optical constants of potassium,

rubidium and cesium for wavelengths less than 2537 Å would provide a further test of Cohen's theory (12) for these metals.

Less is known about the optical properties of lithium than of the other alkali metals. The plasma wavelength of lithium has been reported to be 2050 Å (4) and also 1550 Å (5). Infrared data (55) indicate stronger interband effects in lithium than in the other alkali metals so the critical-angle method may not be applicable for Li.

The extinction coefficients of sodium, potassium, rubidium, and cesium may be measured for wavelengths less than 1700 Å by using hemi-cylinders made of materials which transmit further into the vacuum-ultraviolet.

APPENDIX

Tracings of reflectance, R, as a function of angle-of-incidence, θ, for a representative selection of wavelengths are shown below. The reflectance scale is calibrated in arbitrary units.
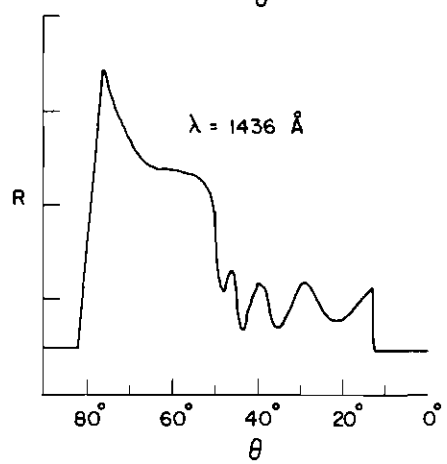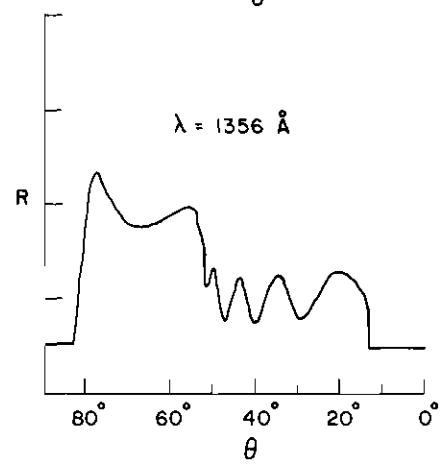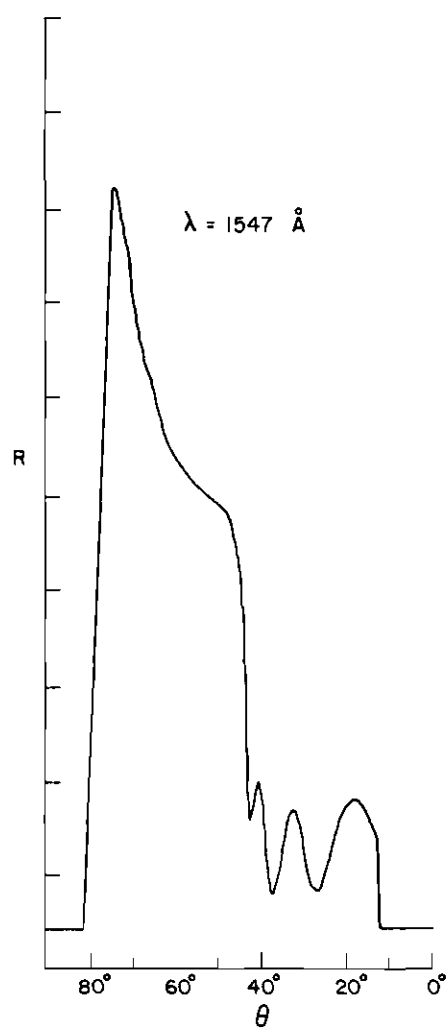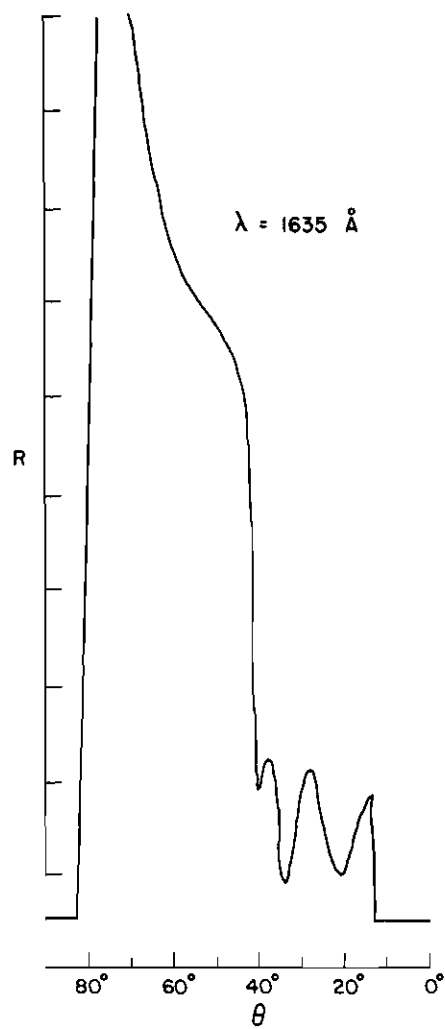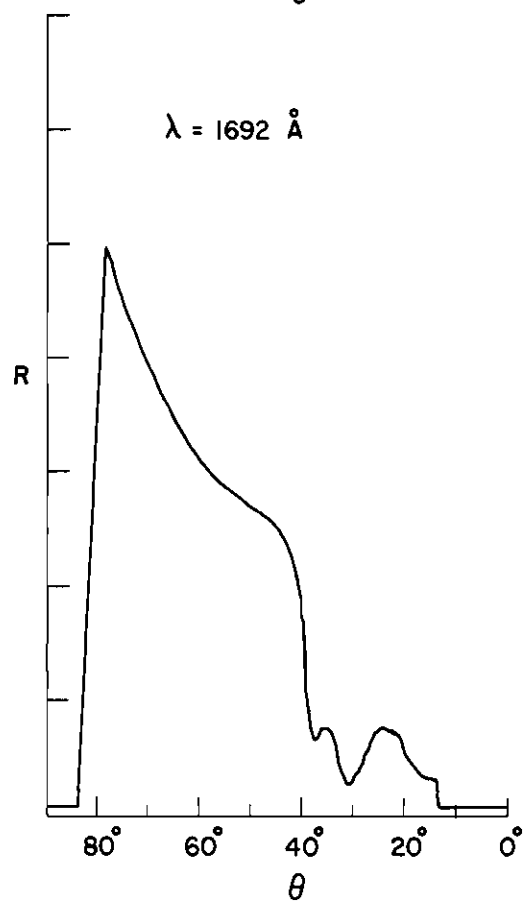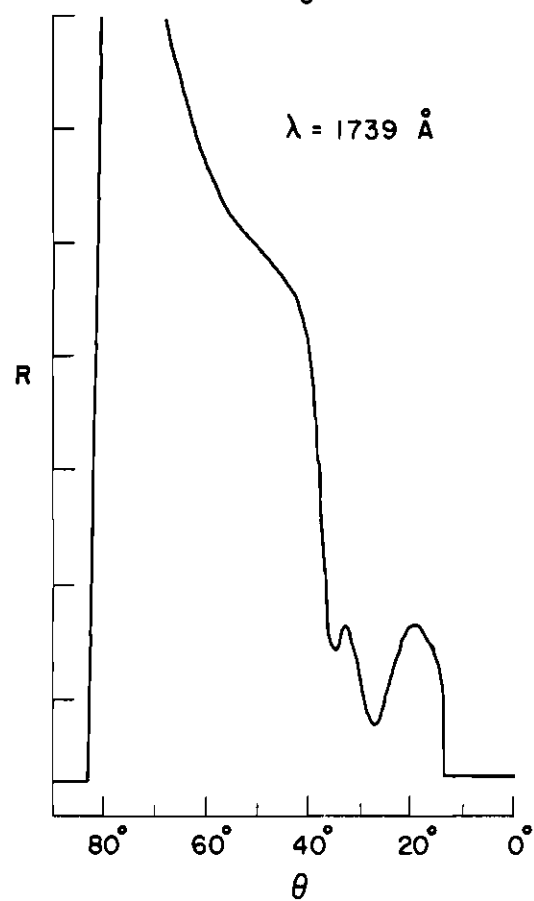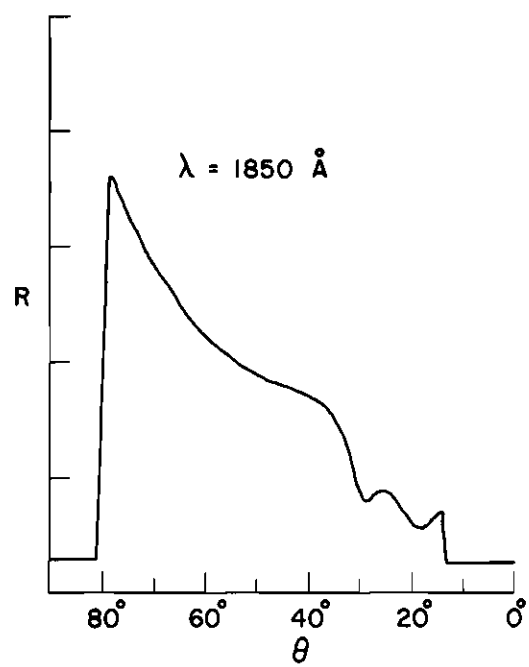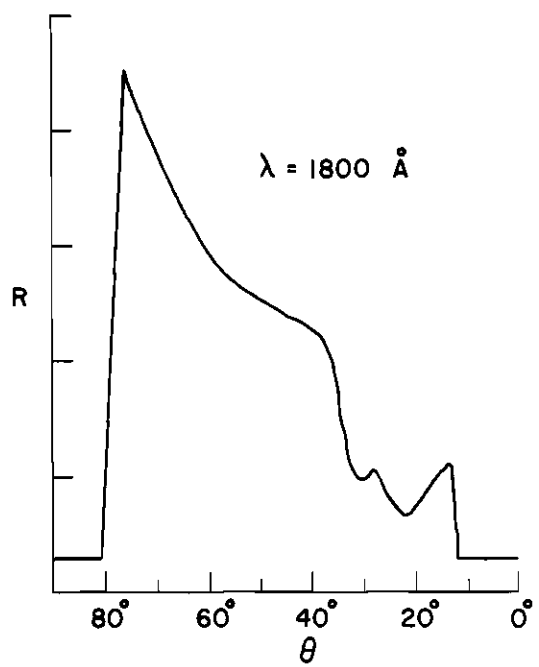
λ = 1119 Å

λ = 1216 Å

λ = 950 Å

λ = 974 Å
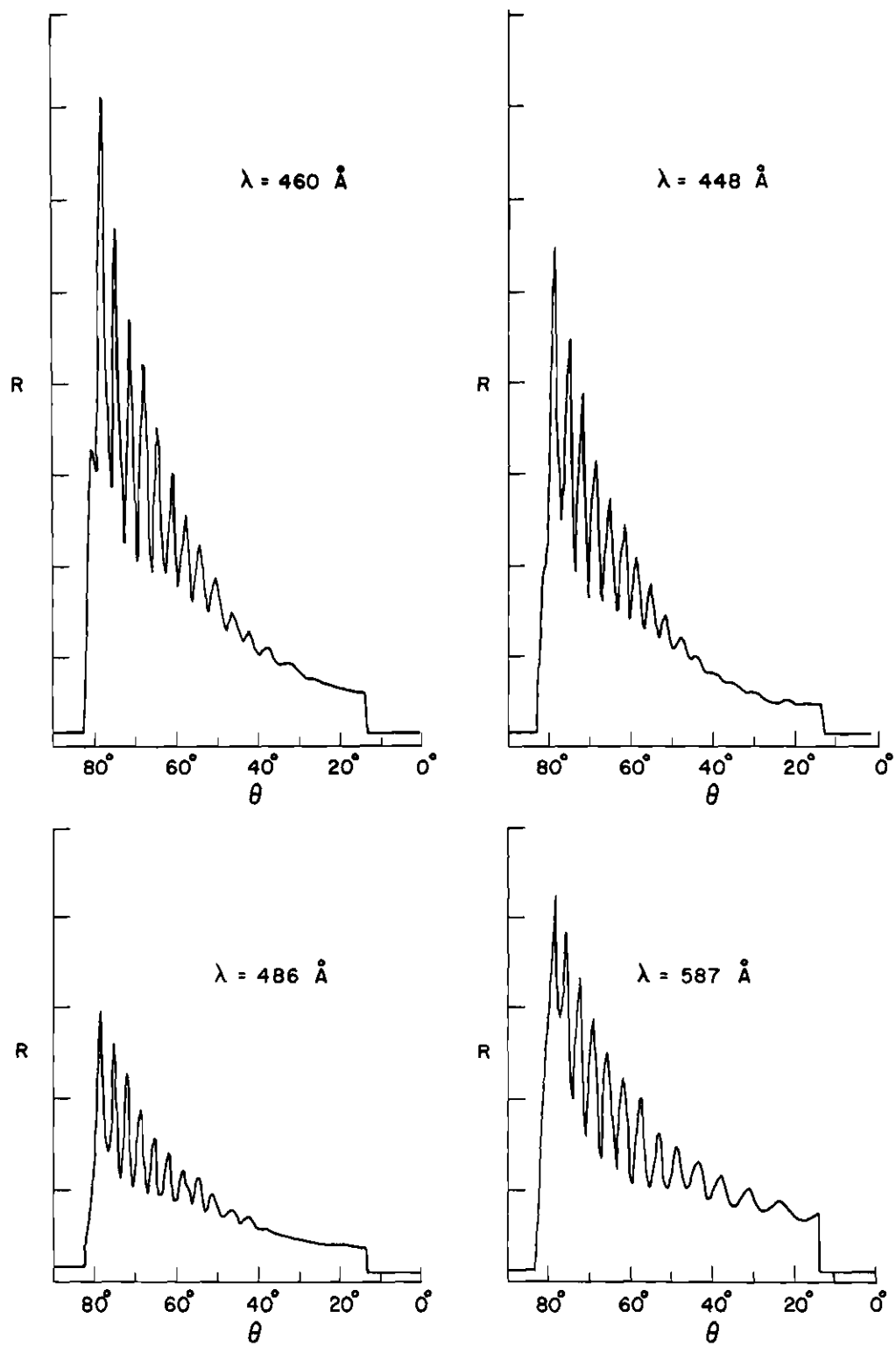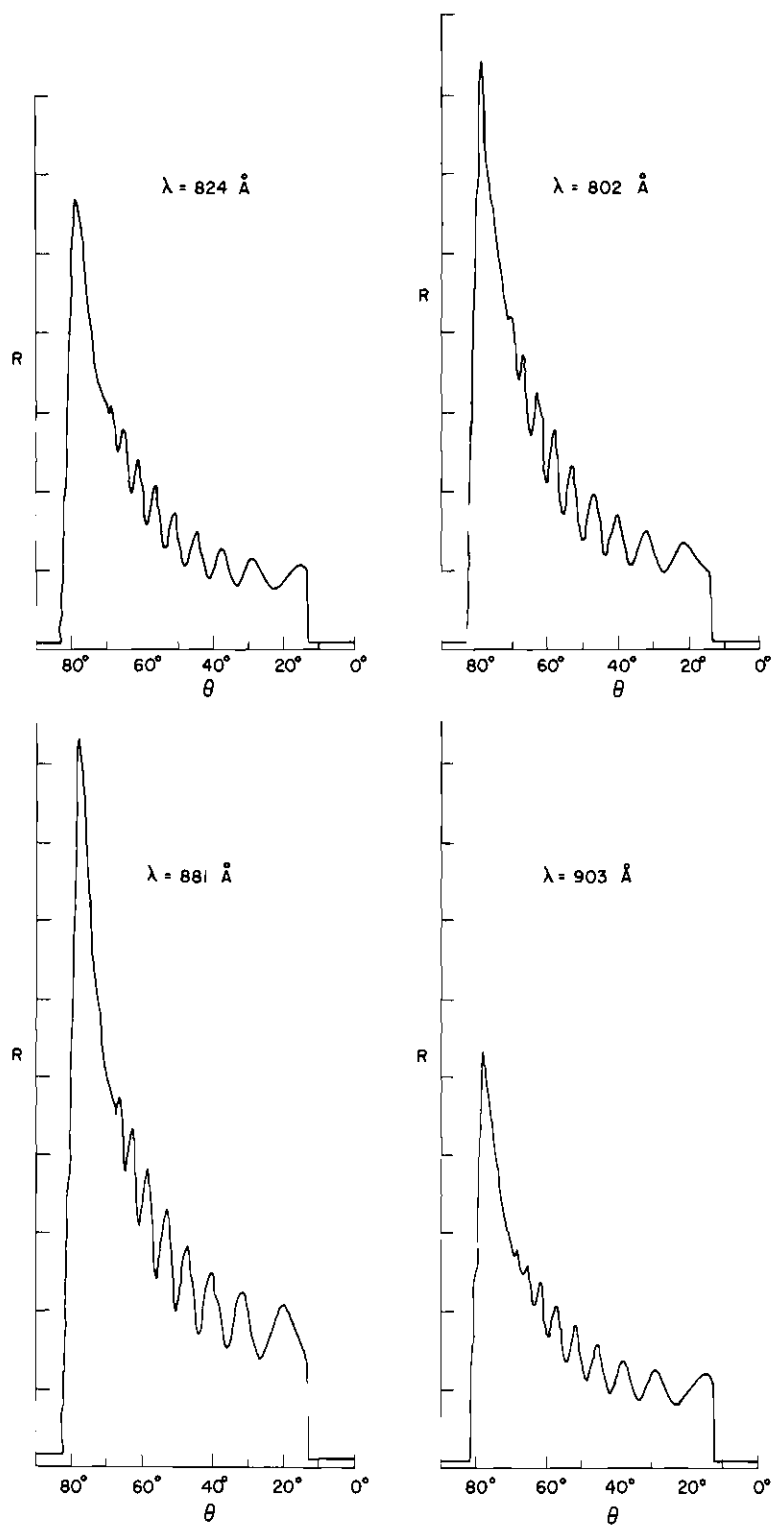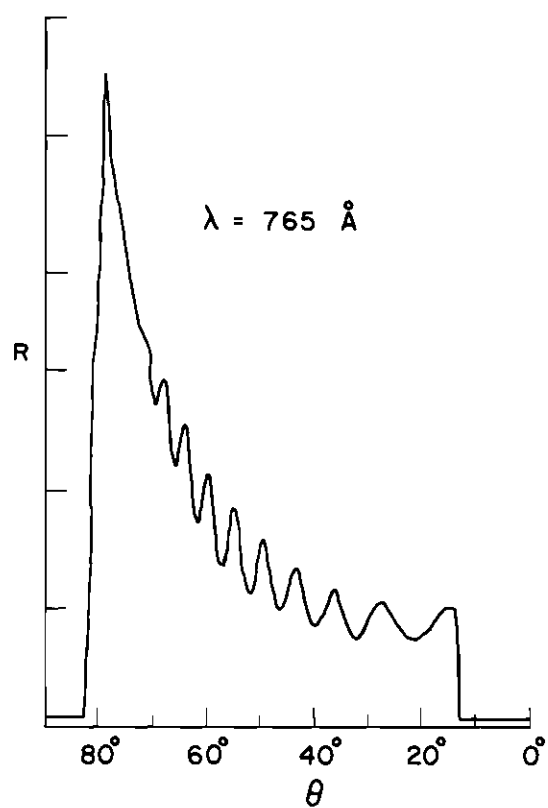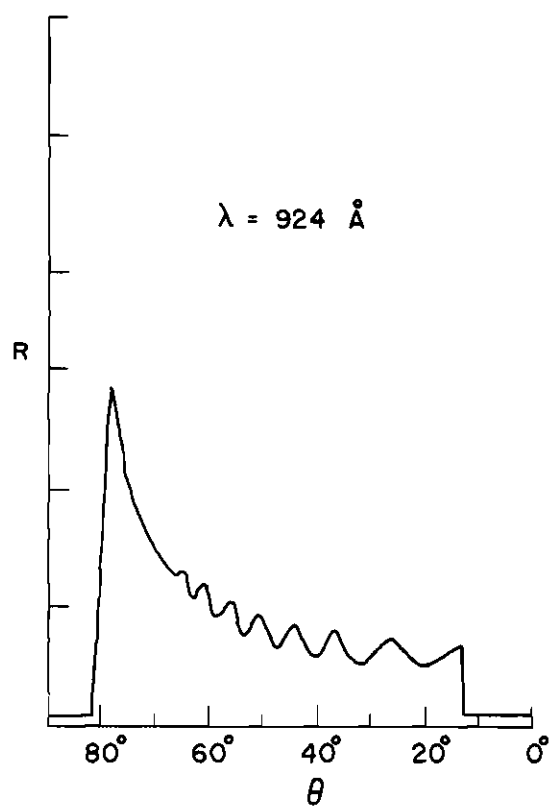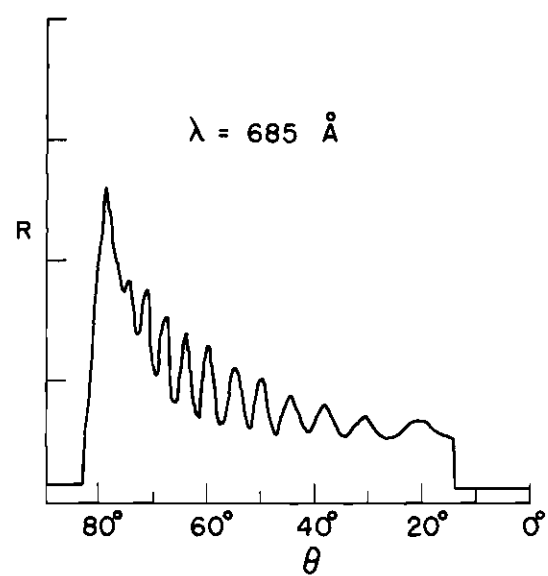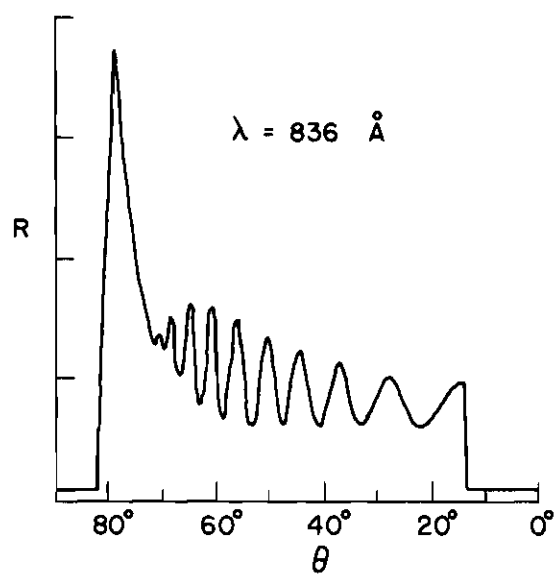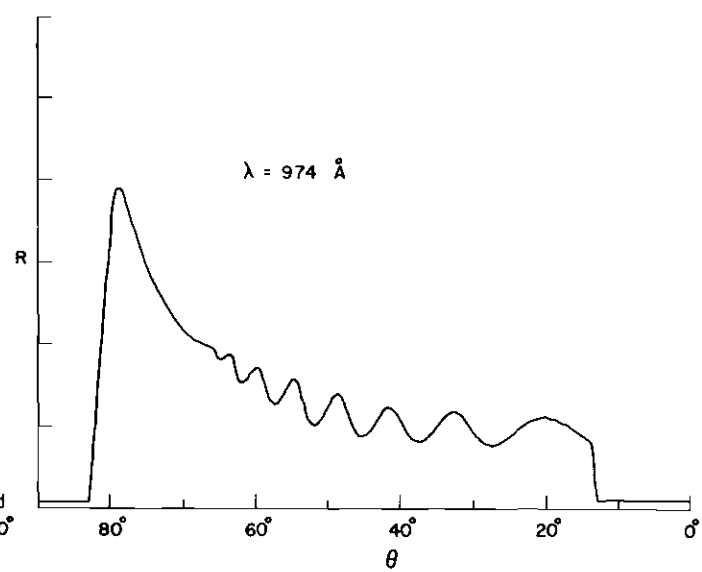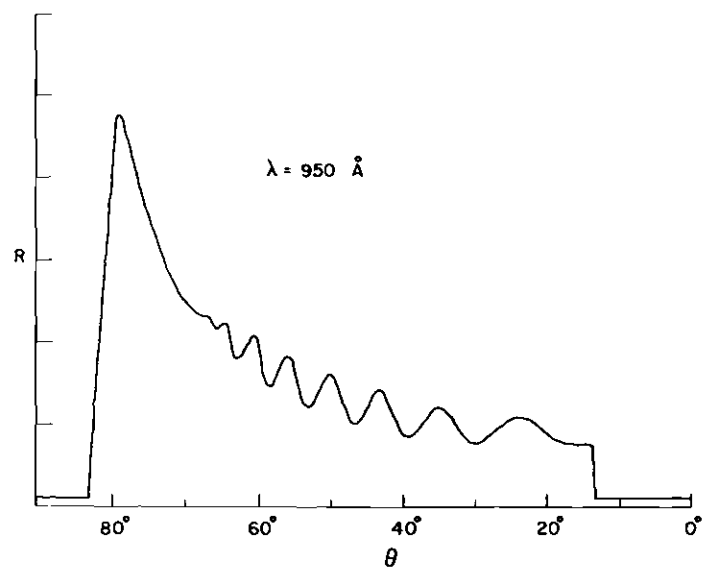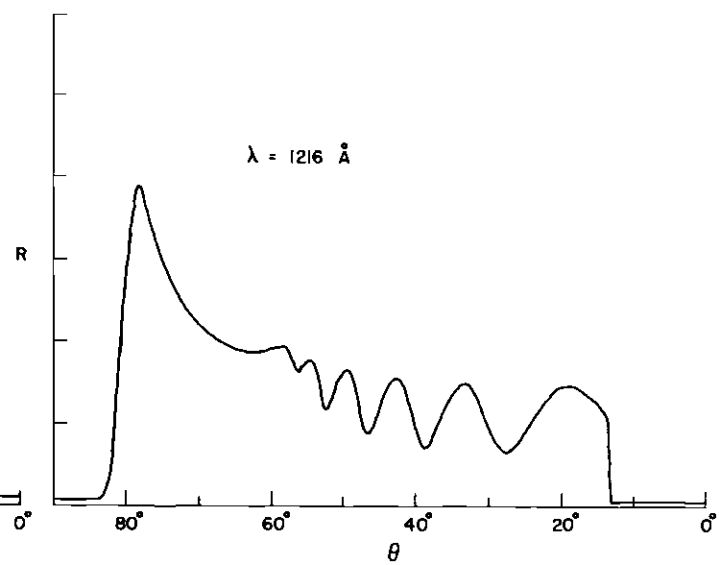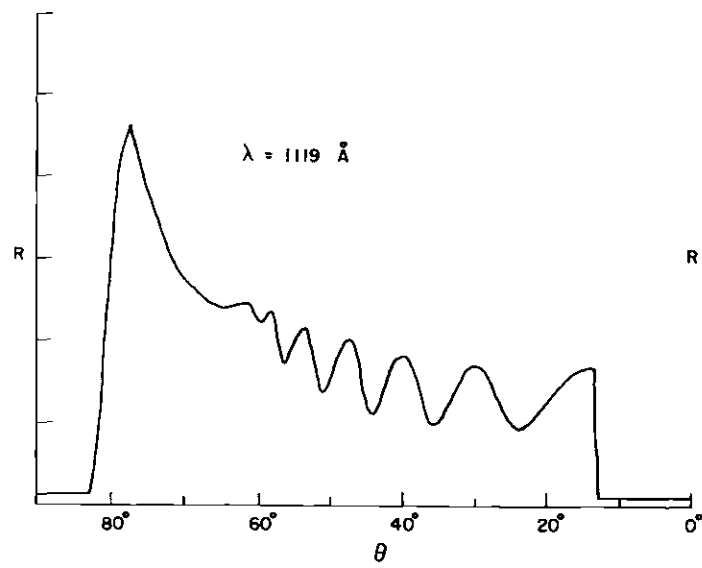
BIBLIOGRAPHY

1. P. Drude, Annalen der Physik 64, 159 (1898).

2. R. W. Duncan and R. C. Duncan, Physical Review 1, 294 (1913).

3. R. W. Wood, Philosophical Magazine 38, 98 (1919).

4. R. W. Wood, Phys. Rev. 44, 353 (1933).

5. R. W. Wood, Nature 131, 582 (1933).

6. R. W. Wood and Charles Lukens, Phys. Rev. 54, 332 (1938).

7. C. Zener, Nature 132, 968 (1933).

8. R. de L. Kronig, Proceedings of the Royal Society (London), 124, 409 (1929); 133, 255 (1931).

9. R. de L. Kronig, Nature 133, 211 (1934).

10. H. E. Ives and H. B. Briggs, Journal of the Optical Society of America 26, 238 (1936); 27, 181 (1937); 27, 395 (1937).

11. H. W. B. Skinner, Philosophical Transactions of the Royal Society of London 239, 95 (1940).

12. M. H. Cohen, Phil. Mag. 3, 762 (1958).

13. J. N. Hodgson, Journal of Physics and Chemistry of Solids 24, 1213 (1963).

14. F. S. Ham, Phys. Rev. 128,82 (1962).

15. A. J. Hughes and Joseph Callaway, Phys. Rev. 136, A1390 (1964).

16. J. F. Kenney, Quarterly Progress Report, Solid State and Molecular Theory Group, M. I. T. , 53, 38 (1964).

17. H. Mayer and B. Hietel, "Experimental Results on the Optical Properties of the Alkali Metals, " in "Optical Properties and Electronic Structure of Metals and Alloys, " ed. F. Abelès, (North-Holland Publishing Co.,

Amsterdam, 1966).

18. H. Mayer and M. H. El Naby, Zeitschrift für Physik, 174, 269 (1963); 174, 280 (1963); 174, 289 (1963).

19. Mansour Moh. Hassab El Naby, Dissertation, der Bergakademie, Clausthal, (1962).

20. Bernhard Hietel, Dissertation, der Bergakademie, Clausthal, (1965).

21. H. Mayer and B. Hietel, Kurznachrichten der Akademie der Wissenschaften; (Göttingen) Nr. 1, p. 1 (1965).

22. M. H. Cohen and J. C. Phillips, Physical Review Letters 12, 662 (1964).

23. M. H. Cohen, Phys. Rev. Letters 12, 664 (1964).

24. M. H. Cohen, "Interpretation of the Optical Properties of the Alkali Metals, " in "Optical Properties and Electronic Structure of Metals and Alloys, " ed. F. Abelès, (North-Holland Publishing Co., Amsterdam, 1966).

25. A. Overhauser, Phys. Rev. Letters 13, 190 (1964).

26. R. A. Ferrell, "Optical Properties of the Alkali Metals, " in "Optical Properties and Electronic Structure of Metals and Alloys, " ed. F. Abelès, (North-Holland Publishing Co., Amsterdam, 1966).

27. J. A. Appelbaum, Phys. Rev. 144, 435 (1966).

28. S. J. Nettel, Phys. Rev. 150, 421 (1966).

29. P. Drude, Ann. der Physik 1, 566 (1900).

30. F. Seitz, "Modern Theory of Solids, " (McGraw-Hill Book Company, Inc., New York, 1940).

31. H. Fröhlich, "Electronen Theorie der Metalle, " (Julius Springer Verlag, Berlin, 1936).

32. D. Bohm and D. Pines, Phys. Rev. 82, 625 (1951); 85, 338 (1952); 92, 609 (1953).

33. D. Pines, "Elementary Excitations in Solids," (W. A. Benjamin, Inc., New York, 1963).

34. N. F. Mott and H. Jones, "The Theory of the Properties of Metals and Alloys," (Clarendon Press, Oxford, 1936).

35. R. A. Ferrell, Phys. Rev. 101, 554 (1956).

36. O. S. Heavens, "Optical Properties of Thin Solid Films," (Dover Publishing Co., New York, 1965).

37. C. E. Moore, National Bureau of Standards Circular 488, Section 1 (1950).

38. J. C. Boyce and H. A. Robinson, J. Opt. Soc. Am. 26, 133 (1936).

39. Kozo Ishiguro and Taizo Sasaki, Scientific Papers of the College of General Education, (University of Tokyo) 12, 19 (1962).

40. Taizo Sasaki and Kozo Ishiguro, Japanese Journal of Applied Physics 2, 289 (1963).

41. F. Stern, "Solid State Physics, Vol. 15," ed. F. Seitz and D. Turnbull, (Academic Press, New York, 1963).

42. W. R. Hunter, Journal of Applied Physics 34, 1565 (1963).

43. R. P. Madden, L. R. Canfield, and G. Hass, J. Opt. Soc. Am. 53, 620 (1963).

44. W. R. Hunter, J. Opt. Soc. Am. 34, 1565 (1963).

45. R. N. Hamm, R. A. MacRae, and E. T. Arakawa, J. Opt. Soc. Am. 55, 1460 (1965).

46. J. L. Robins and P. E. Best, Proceedings of the Physical Society, (London) 79, 110 (1962).

47. J. B. Swan, Phys. Rev. 135, A1467 (1964).

48. C. Kunz, Physical Letters 15, 312 (1965).

49. O. Sueoka, Journal of the Physical Society of Japan 20, 2249 (1965).

50. C. J. Powell, Proc. Phys. Soc. (London) 76, 593 (1960).

51. J. R. Tessman, A. H. Kahn, and W. Shockly, Phys. Rev. 92, 890 (1953).

52. M. Born and W. Heisenberg, Z. Physik 23, 388 (1924).

53. K. Fajans and G. Joos, Z. Physik 23, 1 (1924).

54. L. Pauling, Proc. Roy. Soc., (London) A114, 191 (1927).

55. J. N. Hodgson, "The Optical Properties and Electronic Structure of Lithium, " in "Optical Properties and Electronic Structure of Metals and Alloys, " ed. F. Abelès, (North-Holland Publishing Co. , Amsterdam, 1966).

VITA

John Clark Sutherland was born in New York City. He received his elementary education in the public schools of New York City, Knoxville, Tennessee, and El Paso, Texas. He graduated from Stuyvesant High School in New York City in 1958. In 1962 he was awarded by the Georgia Institute of Technology the degree of Bachelor of Science in Physics (with highest honors). He received the Master of Science in Physics in 1964 also from the Georgia Institute of Technology.